J|A|C|S
ARTICLES
Published on Web 08/15/2002

3D TEDOR NMR Experiments for the Simultaneous Measurement of Multiple Carbon−Nitrogen Distances in Uniformly ^{13}C,^{15}N-Labeled Solids

Christopher P. Jaroniec, Claudiu Filip,† and Robert G. Griffin*

Contribution from the Department of Chemistry and Francis Bitter Magnet Laboratory, Massachusetts Institute of Technology, Cambridge, Massachusetts 02139

Received April 1, 2002

Abstract: We describe three-dimensional magic-angle-spinning NMR experiments for the simultaneous measurement of multiple carbon−nitrogen distances in uniformly ^{13}C,^{15}N-labeled solids. The approaches employ transferred echo double resonance (TEDOR) for $^{13}C-^{15}N$ coherence transfer and ^{15}N and ^{13}C frequency labeling for site-specific resolution, and build on several previous 3D TEDOR techniques. The novel feature of the 3D TEDOR pulse sequences presented here is that they are specifically designed to circumvent the detrimental effects of homonuclear $^{13}C-^{13}C$ *J*-couplings on the measurement of weak $^{13}C-^{15}N$ dipolar couplings. In particular, homonuclear *J*-couplings lead to two undesirable effects: (i) they generate anti-phase and multiple-quantum (MQ) spin coherences, which lead to spurious cross-peaks and phase-twisted lines in the 2D $^{15}N-^{13}C$ correlation spectra, and thus degrade the spectral resolution and prohibit the extraction of reliable cross-peak intensities, and (ii) they significantly reduce cross-peak intensities for strongly *J*-coupled ^{13}C sites (e.g., CO and C^{α}). The first experiment employs *z*-filter periods to suppress the anti-phase and MQ coherences and generates 2D spectra with purely absorptive peaks for all TEDOR mixing times. The second approach uses band-selective ^{13}C pulses to refocus *J*-couplings between ^{13}C spins within the selective pulse bandwidth and ^{13}C spins outside the bandwidth. The internuclear distances are extracted by using a simple analytical model, which accounts explicitly for multiple spin−spin couplings contributing to cross-peak buildup. The experiments are demonstrated in two U-^{13}C,^{15}N-labeled peptides, *N*-acetyl-L-Val-L-Leu (N-ac-VL) and *N*-formyl-L-Met-L-Leu-L-Phe (N-f-MLF), where 20 and 26 $^{13}C-^{15}N$ distances up to ∼5−6 Å were measured, respectively. Of the measured distances, 10 in N-ac-VL and 13 in N-f-MLF are greater than 3 Å and provide valuable structural constraints.

Introduction

Recent advances in magic-angle-spinning (MAS) solid-state nuclear magnetic resonance (SSNMR) instrumentation and methodology[1−3] have greatly extended the applicability of SSNMR from selectively to multiply ^{13}C,^{15}N-labeled peptides and proteins. At moderate magnetic field strengths of 7−14 T (^{1}H Larmor frequencies of 300−600 MHz), complete sequence-specific ^{13}C and ^{15}N resonance assignments have been obtained for several uniformly ^{13}C,^{15}N-labeled microcrystalline peptides[4,5] and peptides that self-assemble to form amyloid fibrils,[6,7] and partial resonance assignments were determined for the 76-residue human ubiquitin.[8,9] At magnetic fields of 17.5−19 T (^{1}H Larmor frequencies of 750−800 MHz), resonance assignments for several uniformly ^{13}C,^{15}N-labeled proteins have been recently presented.[10−13] Specifically, partial assignments have been obtained for the 58-residue bovine pancreatic trypsin inhibitor (BPTI)[10] and the 150 kDa LH2 light-harvesting membrane−protein complex,[11] and nearly complete sequence-specific ^{13}C and ^{15}N[12] and nonexchangeable ^{1}H[13] assignments have been reported for the 62-residue α-spectrin SH3 domain.

Site-specific resonance assignments are a source of valuable structural information in biomolecular solution- and solid-state NMR because the difference between the experimentally

* To whom correspondence should be addressed. E-mail: rgg@mit.edu.
† On leave from National Institute for Research and Development of Isotopic and Molecular Technologies, R-3400 Cluj, Romania.

(1) Bennett, A. E.; Griffin, R. G.; Vega, S. In *Solid State NMR IV: Methods and Applications of Solid-State NMR*; Blumich, B., Ed.; Springer-Verlag: Berlin, 1994; Vol. 33, pp 1−77.
(2) Griffin, R. G. *Nat. Struct. Biol.* **1998**, *5*, 508−512.
(3) Dusold, S.; Sebald, A. *Annu. Rep. Nucl. Magn. Reson. Spectrosc.* **2000**, *41*, 185−264.
(4) Rienstra, C. M.; Hohwy, M.; Hong, M.; Griffin, R. G. *J. Am. Chem. Soc.* **2000**, *122*, 10979−10990.
(5) Detken, A.; Hardy, E. H.; Ernst, M.; Kainosho, M.; Kawakami, T.; Aimoto, S.; Meier, B. H. *J. Biomol. NMR* **2001**, *20*, 203−221.
(6) Balbach, J. J.; Ishii, Y.; Antzutkin, O. N.; Leapman, R. D.; Rizzo, N. W.; Dyda, F.; Reed, J.; Tycko, R. *Biochemistry* **2000**, *39*, 13748−13759.
(7) Jaroniec, C. P.; MacPhee, C. E.; Astrof, N. S.; Zurdo, J.; Dobson, C. M.; Griffin, R. G. *Abstracts of Papers*, 223rd National Meeting of the American Chemical Society, Orlando, FL, Spring 2002; American Chemical Society: Washington, DC, 2002.
(8) Straus, S. K.; Bremi, T.; Ernst, R. R. *J. Biomol. NMR* **1998**, *12*, 39−50.
(9) Hong, M. *J. Biomol. NMR* **1999**, *15*, 1−14.
(10) McDermott, A.; Polenova, T.; Bockmann, A.; Zilm, K. W.; Paulsen, E. K.; Martin, R. W.; Montelione, G. T. *J. Biomol. NMR* **2000**, *16*, 209−219.
(11) Egorova-Zachernyuk, T. A.; Hollander, J.; Fraser, N.; Gast, P.; Hoff, A. J.; Cogdell, R.; de Groot, H. J. M.; Baldus, M. *J. Biomol. NMR* **2001**, *19*, 243−253.
(12) Pauli, J.; Baldus, M.; van Rossum, B.; de Groot, H.; Oschkinat, H. *ChemBiochem* **2001**, *2*, 272−281.
(13) van Rossum, B. J.; Castellani, F.; Rehbein, K.; Pauli, J.; Oschkinat, H. *ChemBiochem* **2001**, *2*, 906−914.

10.1021/ja026385y CCC: $22.00

observed isotropic chemical shifts and the corresponding random coil values can be used to predict the conformation of the protein backbone.[14−20] Additional information about secondary and tertiary structure in solid-phase peptides and proteins can be obtained from direct measurements of homo- and heteronuclear dipolar couplings, reintroduced during MAS by using dipolar recoupling techniques.[1−3] The experiments used for sequential resonance assignments generally exploit the strongest spin−spin interactions and are relatively straightforward to implement in uniformly ^{13}C,^{15}N-labeled systems. On the other hand, long-range distance measurements in these systems are more complicated. The nuclei form a tightly coupled network via through-space (dipolar coupling) and through-bond (*J*-coupling) spin−spin interactions; consequently, the strongest couplings can interfere with the accurate determination of the weaker ones.[21−25] In the following, we will focus our attention on the problem of heteronuclear $^{13}C-^{15}N$ recoupling in multiple-spin systems, with the ultimate goal of measuring multiple carbon−nitrogen distances simultaneously in uniformly ^{13}C,^{15}N-labeled peptides and proteins.

A number of experiments have been developed to reintroduce the dipolar coupling between a pair of low-γ spin $I = {}^1/_2$ nuclei (e.g., ^{13}C, ^{15}N, ^{31}P) during MAS.[1−3] Some of the most robust and versatile heteronuclear recoupling experiments are derived from rotational echo double resonance (REDOR)[26,27] and the closely related transferred echo double resonance (TEDOR).[28,29] (Applications of these methods to systems of importance in biology and materials science have been summarized in several recent reviews.[1−3,30]) During REDOR,[26,27] the $I-S$ dipolar coupling is reintroduced by a train of rotor-synchronized 180° pulses applied to the *S*-spins. This results in the dephasing of the *I*-spin−echo with a modulation frequency proportional to the magnitude of the dipolar coupling. TEDOR[28,29] (the basic pulse sequence consists of two REDOR periods bracketing a pair of 90° pulses on *I*- and *S*-spins) acts to transfer magnetization between dipolar coupled *I* and *S* nuclei, where the buildup of the *S*-spin magnetization is proportional to the magnitude of the $I-S$ dipolar coupling. TEDOR coherence transfer dynamics are analogous to the well-known solution-state INEPT experiment,[31] which uses the heteronuclear *J*-coupling to achieve coherence transfer, and solid-state INEPT experiments,[32] for which coherence transfer is accomplished via heteronuclear dipolar couplings. While REDOR and TEDOR are both well-established for selectively ^{13}C,^{15}N-labeled samples, their application to multiply labeled systems is less straightforward. Depending on the details of the particular experiment, the recoupling dynamics can depend on multiple spin−spin couplings and their relative orientations, which potentially complicates accurate measurements of weak $^{13}C-^{15}N$ dipolar couplings.[24]

Various experiments based on REDOR and TEDOR have been proposed to circumvent the problems associated with multiple-spin systems.[33−46] Most recently, we described a frequency-selective REDOR (FSR)[43] experiment and demonstrated its applications to uniformly ^{13}C,^{15}N-labeled peptides and proteins.[43,47] The experiment was specifically developed to perform accurate site-specific measurements of weak $^{13}C-^{15}N$ dipolar couplings in U-^{13}C,^{15}N-labeled samples. Accordingly, for a tripeptide *N*-formyl-L-Met-L-Leu-L-Phe (N-f-MLF), 16 $^{13}C-^{15}N$ distances up to ∼6 Å were measured by using FSR with ∼0.1−0.3 Å precision[43] and used in combination with multiple dihedral angle constraints[48] to calculate the three-dimensional high-resolution structure of N-f-MLF.[49] In the special case of a biological macromolecule exhibiting sufficient ^{13}C and ^{15}N chemical shift resolution, frequency-selective REDOR was applied to a 248-residue membrane protein, bacteriorhodopsin, to determine two distances between the retinal Schiff base nitrogen and carboxyl groups of aspartate residues, D85 and D212, across the active site.[47]

In the following we discuss three-dimensional heteronuclear correlation (HETCOR) experiments, which are designed to *simultaneously* measure multiple long-range carbon−nitrogen distances in uniformly ^{13}C,^{15}N-labeled samples. During a 3D HETCOR experiment, a series of 2D $I-S$ chemical shift correlation spectra are recorded as a function of the duration of the $I-S$ coherence transfer period (also referred to as the mixing time); for distance measurements the coherence transfer proceeds via $I-S$ dipolar couplings. Cross-peaks located at $(\Omega_{S_j},\Omega_{I_i})$ in the 2D spectra, where Ω_{I_i} and Ω_{S_j} are the isotropic chemical shifts of the *i*th *I*-spin and the *j*th *S*-spin, respectively, are observed only for $I-S$ spin pairs having a sufficiently strong dipolar coupling, and the buildup of cross-peak intensities as a function of the mixing time provides information about $I-S$ distances in a site-specific fashion. The experiments discussed here employ TEDOR for $^{13}C-^{15}N$ coherence transfer and build

(14) Spera, S.; Bax, A. *J. Am. Chem. Soc.* **1991**, *113*, 5490−5492.
(15) Wishart, D. S.; Sykes, B. D. *Methods Enzymol.* **1994**, *239*, 363−392.
(16) Wishart, D. S.; Bigam, C. G.; Holm, A.; Hodges, R. S.; Sykes, B. D. *J. Biomol. NMR* **1995**, *5*, 67−81.
(17) Cornilescu, G.; Delaglio, F.; Bax, A. *J. Biomol. NMR* **1999**, *13*, 289−302.
(18) Saito, H. *Magn. Reson. Chem.* **1986**, *24*, 835−852.
(19) Saito, H.; Tuzi, S.; Naito, A. *Annu. Rep. Nucl. Magn. Reson. Spectrosc.* **1998**, *36*, 79−121.
(20) Luca, S.; Filippov, D. V.; van Boom, J. H.; Oschkinat, H.; de Groot, H. J. M.; Baldus, M. *J. Biomol. NMR* **2001**, *20*, 325−331.
(21) Costa, P. R. Ph.D. Thesis, Massachusetts Institute of Technology, 1996.
(22) Hohwy, M.; Rienstra, C. M.; Jaroniec, C. P.; Griffin, R. G. *J. Chem. Phys.* **1999**, *110*, 7983−7992.
(23) Ladizhansky, V.; Vega, S. *J. Chem. Phys.* **2000**, *112*, 7158−7168.
(24) Fyfe, C. A.; Lewis, A. R. *J. Phys. Chem. B* **2000**, *104*, 48−55.
(25) Hodgkinson, P.; Emsley, L. *J. Magn. Reson.* **1999**, *139*, 46−59.
(26) Gullion, T.; Schaefer, J. *J. Magn. Reson.* **1989**, *81*, 196−200.
(27) Gullion, T.; Schaefer, J. *Adv. Magn. Reson.* **1989**, *13*, 57−83.
(28) Hing, A. W.; Vega, S.; Schaefer, J. *J. Magn. Reson.* **1992**, *96*, 205−209.
(29) Hing, A. W.; Vega, S.; Schaefer, J. *J. Magn. Reson. A* **1993**, *103*, 151−162.
(30) McDowell, L. M.; Schaefer, J. *Curr. Opin. Struct. Biol.* **1996**, *6*, 624−629.
(31) Morris, G. A.; Freeman, R. *J. Am. Chem. Soc.* **1979**, *101*, 760−762.
(32) Roberts, J. E.; Vega, S.; Griffin, R. G. *J. Am. Chem. Soc.* **1984**, *106*, 2506−2512.
(33) Fyfe, C. A.; Mueller, K. T.; Grondey, H.; Wong-Moon, K. C. *Chem. Phys. Lett.* **1992**, *199*, 198−204.
(34) van Eck, E. R. H.; Veeman, W. S. *J. Magn. Reson. A* **1994**, *109*, 250−252.
(35) Michal, C. A.; Jelinski, L. W. *J. Am. Chem. Soc.* **1997**, *119*, 9059−9060.
(36) Bennett, A. E.; Becerra, L. R.; Griffin, R. G. *J. Chem. Phys.* **1994**, *100*, 812−814.
(37) Bennett, A. E.; Rienstra, C. M.; Lansbury, P. T.; Griffin, R. G. *J. Chem. Phys.* **1996**, *105*, 10289−10299.
(38) Schaefer, J. *J. Magn. Reson.* **1999**, *137*, 272−275.
(39) Gullion, T.; Pennington, C. H. *Chem. Phys. Lett.* **1998**, *290*, 88−93.
(40) Liivak, O.; Zax, D. B. *J. Chem. Phys.* **2000**, *113*, 1088−1096.
(41) Liivak, O.; Zax, D. B. *J. Chem. Phys.* **2001**, *115*, 402−409.
(42) Jaroniec, C. P.; Tounge, B. A.; Rienstra, C. M.; Herzfeld, J.; Griffin, R. G. *J. Am. Chem. Soc.* **1999**, *121*, 10237−10238.
(43) Jaroniec, C. P.; Tounge, B. A.; Herzfeld, J.; Griffin, R. G. *J. Am. Chem. Soc.* **2001**, *123*, 3507−3519.
(44) Chan, J. C. C.; Eckert, H. *J. Magn. Reson.* **2000**, *147*, 170−178.
(45) Chan, J. C. C. *Chem. Phys. Lett.* **2001**, *335*, 289−297.
(46) Chan, J. C. C.; Eckert, H. *J. Chem. Phys.* **2001**, *115*, 6095−6105.
(47) Jaroniec, C. P.; Lansing, J. C.; Tounge, B. A.; Belenky, M.; Herzfeld, J.; Griffin, R. G. *J. Am. Chem. Soc.* **2001**, *123*, 12929−12930.
(48) Rienstra, C. M.; Hohwy, M.; Mueller, L. J.; Jaroniec, C. P.; Reif, B.; Griffin, R. G. *J. Am. Chem. Soc.* **2002**, in press.
(49) Rienstra, C. M.; Tucker-Kellogg, L.; Jaroniec, C. P.; Hohwy, M.; Reif, B.; McMahon, M. T.; Tidor, B.; Lozano-Perez, T.; Griffin, R. G. *Proc. Natl. Acad. Sci. U.S.A.* **2002**, *99*, 10260−10265.

on 3D TEDOR techniques described previously by Fyfe and co-workers,[33] van Eck and Veeman,[34] and Michal and Jelinski.[35] We note that a 3D HETCOR experiment of this type based on band-selective $^{13}C-^{15}N$ cross-polarization[4,50] has also been discussed.[51]

The previous 3D TEDOR pulse sequences,[33,34] where the initial *S*-spin magnetization is frequency labeled and transferred by using TEDOR to the *I*-spins for detection, are not directly applicable to uniformly ^{13}C,^{15}N-labeled systems, because $^{13}C-^{13}C$ dipolar and/or ^{13}C and ^{15}N chemical shift anisotropy (CSA) interactions are active during the mixing period and interfere with the $^{13}C-^{15}N$ coherence transfer process. These 3D TEDOR experiments were recently extended to multiple ^{13}C,^{15}N spin systems by Michal and Jelinski,[35] who described an approach where the initial ^{13}C magnetization is transferred to ^{15}N for frequency labeling and subsequently transferred back to ^{13}C for detection; the resulting experiment is relatively insensitive to strong $^{13}C-^{13}C$ dipolar couplings and significant ^{13}C and ^{15}N CSA interactions. While this modified 3D TEDOR experiment[35] addresses many of the problems associated with uniformly ^{13}C,^{15}N-labeled samples, it is not explicitly compensated for homonuclear $^{13}C-^{13}C$ *J*-couplings ($J = 30-60$ Hz in peptides[52]), which interfere with the measurement of weak $^{13}C-^{15}N$ dipolar couplings. These homonuclear *J*-couplings generate anti-phase and multiple-quantum (MQ) spin coherences during the mixing period, which lead to spurious cross-peaks and phase-twisted lines in the 2D spectra, and prohibit the extraction of reliable cross-peak intensities. These problems become particularly severe for mixing times on the order of $t_{mix} \approx 1/(2J)$. Furthermore, the cross-peaks are modulated by the *J*-evolution, which leads to significantly reduced intensities for strongly *J*-coupled ^{13}C sites (e.g., CO and C^{α}).

In this paper, we describe two modified 3D TEDOR experiments specifically designed to address the problems associated with the homonuclear *J*-couplings. The first approach employs *z*-filter periods to suppress the anti-phase and MQ coherences, generates 2D $^{15}N-^{13}C$ correlation spectra with pure absorption mode peaks for all TEDOR mixing times, and provides information about all carbon−nitrogen distances simultaneously. The second approach uses band-selective ^{13}C pulses to refocus *J*-couplings between ^{13}C spins within the selective pulse bandwidth and ^{13}C spins outside the bandwidth and is particularly applicable to distance measurements involving strongly *J*-coupled ^{13}C sites (homonuclear *J*-decoupling of this type has been used previously in solution- and solid-state NMR experiments[42,43,53,54]). The $^{13}C-^{15}N$ distances are extracted by using a simple analytical model, which accounts explicitly for multiple spin−spin interactions contributing to cross-peak buildup. The methods are demonstrated in model U-^{13}C,^{15}N-labeled peptides, *N*-acetyl-L-Val-L-Leu and *N*-formyl-L-Met-L-Leu-L-Phe, where 20 and 26 $^{13}C-^{15}N$ distances up to ∼5−6 Å were measured, respectively.

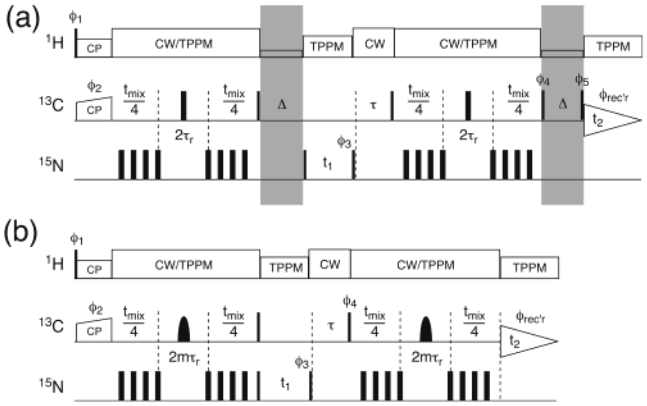

Figure 1. 3D *z*-filtered TEDOR (a) and 3D band-selective TEDOR (b) pulse sequences. Narrow and wide solid rectangles represent $\pi/2$ and π pulses, respectively. During REDOR, two π pulses per rotor period are applied on the ^{15}N channel and phase cycled according to the *xy*-4 scheme.[56] The short delay, τ, ensures that the total delay between the REDOR mixing periods is equal to an integer number of rotor cycles and is required for efficient reconversion of anti-phase coherences into observable ^{13}C magnetization. In (a), the modifications to the recently described 3D TEDOR experiment[35] are highlighted by gray rectangles. The modifications consist of two *z*-filter periods, Δ, which eliminate multiple-quantum and anti-phase spin coherences generated by $^{13}C-^{13}C$ *J*-evolution (see text for details). During the *z*-filters, a weak proton rf field, $\omega_{rf} \approx \omega_r$, was applied[57] to facilitate the rapid dephasing of transverse ^{13}C spin coherences via the contact with the abundant proton bath. In (b), band-selective ^{13}C Gaussian π pulses refocus $^{13}C-^{13}C$ *J*-couplings to nuclei outside the π pulse bandwidth. The phase cycles were as follow: (a) $\phi_1 = 16\times(1)\ 16\times(3)$, $\phi_2 = 1$, $\phi_3 = 13$, $\phi_4 = 2244$, $\phi_5 = 11112222\ 33334444$, $\phi_{rec'r} = 42241331\ 24423113\ 24423113\ 42241331$; (b) $\phi_1 = 8\times(1)\ 8\times(3)$, $\phi_2 = 1$, $\phi_3 = 13$, $\phi_4 = 11223344$, $\phi_{rec'r} = 31241342\ 13423124$, where $1 = x$, $2 = y$, $3 = -x$, $4 = -y$. All remaining pulses (except ^{15}N π pulses during REDOR which were phase cycled $xy - 4$ and ^1H spin-lock which had phase *y*) have phase *x*. Hypercomplex data were acquired by shifting ϕ_3 according to Ruben and co-workers.[58]

Experimental Section

NMR Experiments. NMR spectra were recorded at 11.7 T (500.1 MHz ^1H, 125.8 MHz ^{13}C, 50.7 MHz ^{15}N) by using a custom-designed spectrometer (courtesy of Dr. David J. Ruben) with a Chemagnetics (Fort Collins, CO) triple-resonance MAS probe. The probe was equipped with a 4.0 mm Chemagnetics spinning module. The spinning frequency of 10.0 kHz was used in the experiments and regulated to ±5 Hz with a Doty Scientific (Columbia, SC) spinning frequency controller. Samples were centerpacked in the rotors to minimize the effects of rf inhomogeneity. The 3D TEDOR pulse sequences are shown in Figure 1 and described in detail in the Theoretical Background section below. Unless otherwise indicated, the ^{15}N REDOR π pulse length was 10 μs, the ^{13}C and ^{15}N $\pi/2$ pulses were 5 μs, the TPPM decoupling was ∼100 kHz (total phase difference, 12°; TPPM pulse length, 5.0 μs) during mixing and ∼83 kHz (total phase difference, 12°; TPPM pulse length, 6.0 μs) during t_1 and t_2, the CW decoupling was 100 kHz, and the ^{13}C band-selective Gaussian pulse (Figure 1b) was 0.4 ms, divided into 64 increments, and truncated at 1% of the maximum amplitude.

U-^{13}C,^{15}N-Labeled Peptides. The peptides used in the experiments were [U-^{13}C,^{15}N]*N*-acetyl-L-Val-L-Leu (N-ac-VL) and *N*-formyl-[U-^{13}C,^{15}N]L-Met-L-Leu-L-Phe (N-f-MLF). The U-^{13}C,^{15}N-labeled amino acids and [1,2-^{13}C]acetic anhydride used in the peptide synthesis were purchased from Cambridge Isotope Laboratories (Andover, MA). N-ac-VL and N-f-MLF were synthesized by Synpep (Dublin, CA) and American Peptide (Sunnyvale, CA), respectively, using standard solid-phase methods and purified by HPLC. To minimize the effects of intermolecular couplings on the measured distances, the U-^{13}C,^{15}N-labeled peptides were diluted in the respective natural abundance peptides followed by recrystallization from appropriate solvents: N-ac-

(50) Baldus, M.; Petkova, A. T.; Herzfeld, J.; Griffin, R. G. *Mol. Phys.* **1998**, *95*, 1197−1207.
(51) Rienstra, C. M. Presented at the 2nd Alpine Conference on Solid-State NMR, Chamonix, France, 2001.
(52) Cavanagh, J.; Fairbrother, W. J.; Palmer, A. G.; Skelton, N. J. *Protein NMR Spectroscopy: Principles and Practice*; Academic Press: San Diego, 1996.
(53) Brüschweiler, R.; Griesinger, C.; Sørensen, O. W.; Ernst, R. R. *J. Magn. Reson.* **1988**, *78*, 178−185.
(54) Straus, S. K.; Bremi, T.; Ernst, R. R. *Chem. Phys. Lett.* **1996**, *262*, 709−715.

VL was diluted to ~20% and crystallized from a 1:1 (v/v) H_2O:acetone solution,[55] and N-f-MLF was diluted to ~10% and crystallized from 2-propanol.[4,43]

Theoretical Background

3D TEDOR Pulse Sequences. The 3D TEDOR experiments are presented in Figure 1. The 3D *z*-filtered TEDOR sequence (Figure 1a) (also denoted in the following as 3D ZF TEDOR) provides information about all $^{13}C-^{15}N$ dipolar couplings simultaneously. The 3D band-selective TEDOR sequence (3D BASE TEDOR) shown in Figure 1b probes dipolar couplings for ^{13}C spins within the selective pulse bandwidth and is particularly applicable to distance measurements involving sites with strong $^{13}C-^{13}C$ *J*-couplings (e.g., CO and C^{α}).

The desired TEDOR coherence transfer pathway for a heteronuclear $I-S$ spin pair (I and S represent ^{13}C and ^{15}N, respectively) with the effective dipolar coupling, ω, is

$$\begin{aligned} I_x &\xrightarrow{\text{REDOR}} 2I_yS_z \sin(\omega t_{\text{mix}}/2) \xrightarrow{90_x(I),90_x(S)} \\ &-2I_zS_y \sin(\omega t_{\text{mix}}/2) \xrightarrow{t_1} \\ &-2I_zS_y \sin(\omega t_{\text{mix}}/2)\, e^{i\Omega_S t_1} \xrightarrow{90_{-x}(I),90_{x/y}(S)} \\ &-2I_yS_z \sin(\omega t_{\text{mix}}/2)\, e^{i\Omega_S t_1} \xrightarrow{\text{REDOR}} \\ I_x \sin^2(\omega t_{\text{mix}}/2)\, e^{i\Omega_S t_1} &\xrightarrow{t_2} I_x \sin^2(\omega t_{\text{mix}}/2)\, e^{i\Omega_S t_1} e^{i\Omega_I t_2} \end{aligned}$$

The transverse *I*-spin (^{13}C) magnetization is created by using ramped cross-polarization from protons.[59] Subsequently, a REDOR sequence,[26,27] initiated for a time $t_{\text{mix}}/2$, reintroduces the $I-S$ dipolar coupling and generates *I*-spin coherence in anti-phase with respect to the *S*-spin ($\sim I_yS_z$). The first pair of 90° pulses on the *I*- and *S*-spins results in coherence transfer to the *S*-spin ($\sim I_zS_y$). This coherence is frequency labeled in t_1 with the *S*-spin chemical shift, Ω_S. The second pair of 90° pulses on the *I*- and *S*-spins transfer the coherence back to the *I*-spin ($\sim I_yS_z$). The resulting anti-phase coherence is reconverted into observable *I*-spin magnetization ($\sim I_x$) during the second REDOR period and frequency labeled with the *I*-spin chemical shift, Ω_I, during the acquisition of the FID in t_2. Assuming quadrature detection in t_1 and t_2,[52,60] a Fourier transformation of the time-domain data results in a 2D spectrum with a cross-peak at the frequency (Ω_S,Ω_I). For each crystallite in the powder sample, the cross-peak intensity is modulated as a function of the mixing time, t_{mix}, according to $\sin^2(\omega t_{\text{mix}}/2)$.

In our implementation of 3D TEDOR experiments for uniformly ^{13}C,^{15}N-labeled samples, all REDOR pulses are applied on the ^{15}N channel to avoid the recoupling of ^{13}C spins[61,62] and phased according to the *xy*-4 scheme[56] to compensate for pulse imperfections and resonance offset effects (pulse timings have been described in detail elsewhere[43]). The MQ and anti-phase terms in the density matrix created by homonuclear *J*-evolution are suppressed by using two *z*-filter periods, Δ, highlighted by gray rectangles. For 3D BASE TEDOR, the band-selective ^{13}C pulse, centered in the period occupying an even number of rotor cycles ($2m\tau_r$), refocuses homonuclear *J*-couplings. The influence of proton couplings during the $^{13}C-^{15}N$ recoupling periods is attenuated by a combination of continuous-wave (CW) and two-pulse phase modulation (TPPM)[63] decoupling, as described in detail previously.[43] TPPM decoupling was used during t_1 and t_2. The delay, τ, following t_1 evolution ensures that the total delay between the REDOR mixing periods is equal to an integral number of rotor cycles and is crucial to the efficient reconversion of anti-phase coherences to observable ^{13}C magnetization.

Spin Dynamics in U-^{13}C,^{15}N-Labeled Systems. We consider a uniformly ^{13}C,^{15}N-labeled sample spinning rapidly about the magic angle ($\theta_m = \tan^{-1}\sqrt{2}$) at a frequency far from rotational resonance conditions.[64] For the 3D TEDOR pulse sequence shown in Figure 1a, the spin system can be considered to evolve under isotropic chemical shifts and homonuclear *J*-couplings during the free evolution periods, t_1 and t_2,

$$H = \sum_k \Omega_{Ik} I_{kz} + \sum_k \Omega_{Sk} S_{kz} + \sum_{j<k} \pi J_{jk} 2I_{jz} I_{kz} \qquad (1)$$

and under the recoupled heteronuclear dipolar interactions and homonuclear *J*-couplings during the two REDOR mixing periods, t_{mix},

$$H = \sum_{j,k} \omega_{jk} 2I_{jz} S_{kz} + \sum_{j<k} \pi J_{jk} 2I_{jz} I_{kz} \qquad (2)$$

In the above expressions, I and S angular momentum operators represent the ^{13}C and ^{15}N spins, respectively, Ω_I and Ω_S are the ^{13}C and ^{15}N isotropic chemical shifts, and J is the $^{13}C-^{13}C$ *J*-coupling constant (in hertz). ω is the orientation-dependent effective $^{13}C-^{15}N$ dipolar coupling reintroduced by the REDOR sequence (a detailed expression for ω can be found in ref 43 and references therein), which is a function of the dipolar coupling constant, D (in hertz), and hence the internuclear distance, r:

$$D = -\left(\frac{\mu_0}{4\pi}\right)\frac{\gamma_I\gamma_S\hbar}{2\pi r^3} \qquad (3)$$

Since all terms in eqs 1 and 2 commute with each other, the time evolution of spin coherences can be derived by using straightforward product-operator calculations.[65] A detailed analysis of the spin dynamics for a simple multiple-spin system (I_2-S) was performed explicitly. Complete results are presented in the Appendix, and the most important points are summarized below. The main conclusion of the analysis is that the presence of a network of multiple *J*-coupled ^{13}C spins causes serious limitations for measuring weak $^{13}C-^{15}N$ dipolar couplings in uniformly ^{13}C,^{15}N-labeled systems by using 3D TEDOR schemes, which are not explicitly compensated for homonuclear *J*-couplings.

(55) Stewart, P. L.; Tycko, R.; Opella, S. J. *J. Chem. Soc., Faraday Trans. 1* **1988**, *84*, 3803−3819.
(56) Gullion, T.; Baker, D. B.; Conradi, M. S. *J. Magn. Reson.* **1990**, *89*, 479−484.
(57) Oas, T. G.; Griffin, R. G.; Levitt, M. H. *J. Chem. Phys.* **1988**, *89*, 692−695.
(58) States, D. J.; Haberkorn, R. A.; Ruben, D. J. *J. Magn. Reson.* **1982**, *48*, 286−292.
(59) Metz, G.; Wu, X.; Smith, S. O. *J. Magn. Reson. A* **1994**, *110*, 219−227.
(60) Ernst, R. R.; Bodenhausen, G.; Wokaun, A. *Principles of Nuclear Magnetic Resonance in One and Two Dimensions*; Clarendon Press: Oxford, 1991.
(61) Gullion, T.; Vega, S. *Chem. Phys. Lett.* **1992**, *194*, 423−428.
(62) Bennett, A. E.; Ok, J. H.; Griffin, R. G.; Vega, S. *J. Chem. Phys.* **1992**, *96*, 8624−8627.
(63) Bennett, A. E.; Rienstra, C. M.; Auger, M.; Lakshmi, K. V.; Griffin, R. G. *J. Chem. Phys.* **1995**, *103*, 6951−6957.
(64) Raleigh, D. P.; Levitt, M. H.; Griffin, R. G. *Chem. Phys. Lett.* **1988**, *146*, 71−76.
(65) Sørensen, O. W.; Eich, G. W.; Levitt, M. H.; Bodenhausen, G.; Ernst, R. R. *Prog. NMR Spectrosc.* **1983**, *16*, 163−192.

To derive the basic spin dynamics for 3D TEDOR experiments, it is sufficient to monitor the evolution of the transverse magnetization for only one of ^{13}C nuclei in the I_2-S system, for instance I_{1x}. During the REDOR mixing period, the initial density operator evolves under the Hamiltonian in eq 2 according to

$$I_{1x} \xrightarrow{\text{REDOR}} I_{1x}c_{\omega 1}c_J + 2I_{1y}I_{2z}c_{\omega 1}s_J + 2I_{1y}S_zs_{\omega 1}c_J - 4I_{1x}I_{2z}S_zs_{\omega 1}s_J \quad (4)$$

where

$$s_{\omega 1} = \sin(\omega_1 t_{\text{mix}}/2)$$

$$c_{\omega 1} = \cos(\omega_1 t_{\text{mix}}/2)$$

$$s_J = \sin(\pi J t_{\text{mix}}/2)$$

$$c_J = \cos(\pi J t_{\text{mix}}/2) \quad (5)$$

and ω_1 and J represent the I_1-S dipolar coupling and the I_1-I_2 J-coupling, respectively.

Equation 4 highlights the fundamental problems associated with the presence of homonuclear J-couplings during REDOR mixing. The initial transverse ^{13}C magnetization evolves not only into ^{13}C$-^{15}$N anti-phase spin coherences ($\sim I_yS_z$), which generate the desired cross-peaks at (Ω_S,Ω_I) in the 2D correlation spectra and give useful information about ^{13}C$-^{15}$N distances, but also into multiple-spin coherences that depend on ^{13}C$-^{13}$C correlations. These are represented by zero-quantum (ZQ) and double-quantum (DQ) coherences with respect to the ^{13}C spin operators ($\sim I_{1x}I_{2y}S_y$) at the end of the first REDOR (excitation) period, followed by 90° pulses on the I and S channels, and by anti-phase coherences ($\sim I_{1y}I_{2z}$) at the end of the second REDOR (reconversion) period. Evolution of these spurious coherences during t_1 and t_2 leads to severe distortions in the resulting 2D spectra. As shown in detail in the Appendix, additional cross-peaks occur in the indirect dimension, and phase-twisted line shapes develop along both spectral dimensions with increasing mixing time. These artifacts, which are not related to $I-S$ dipolar couplings, degrade the spectral resolution and prohibit the extraction of reliable cross-peak intensities.

Two improved 3D TEDOR schemes are proposed to compensate for the detrimental effects of homonuclear J-couplings. In the 3D ZF TEDOR pulse sequence (Figure 1a), the spurious cross-peaks and phase-twisted line shapes are suppressed by inserting two z-filters (highlighted by gray rectangles) prior to t_1 and t_2 free evolution periods. During the filtering periods, the spin coherences which give purely absorptive lines are stored longitudinally, while those responsible for the occurrence of anti-phase signals remain in the transverse plane and are rapidly dephased through the interaction with the abundant proton bath. The resulting 2D spectra contain a purely absorptive cross-peak located at (Ω_{N_j},Ω_{C_i}) for each dipolar coupled carbon$-$nitrogen spin pair, C_i-N_j. The cross-peak intensity is given by

$$V_{ij}(t_{\text{mix}}) = V_i(0)\langle \sin^2(\omega_{ij}t_{\text{mix}}/2) \prod_{k=1\neq j}^{N_i} \cos^2(\omega_{ik}t_{\text{mix}}/2)\rangle \prod_{l=1\neq i}^{m_i} \cos^2(\pi J_{il}t_{\text{mix}}/2) \quad (6)$$

Here, $V_i(0)$ is the reference intensity for the ith ^{13}C spin in the one-dimensional cross-polarization experiment, ω_{ij} is the active ^{13}C$-^{15}$N dipolar coupling which generates the cross-peak located at (Ω_{N_j},Ω_{C_i}), N_i is the number of ^{15}N spins simultaneously coupled to the ith ^{13}C nucleus, the summation index k runs over n_i passive dipolar couplings, ω_{ik}, where $n_i = N_i - 1$, $\langle ... \rangle$ represents the average over different crystallites in the powder, and the summation index l runs over m_i ^{13}C spins J-coupled to the ith ^{13}C spin. We note that for an isolated $I-S$ spin pair with no I-spin J-coupling partners and in the absence of relaxation, the maximum achievable cross-peak intensity is approximately 52% of the reference cross-polarization intensity.[29] In a model spin pair, [2-^{13}C,^{15}N]glycine with $D \approx 900$ Hz, we have achieved a TEDOR coherence transfer efficiency of ~45% of the cross-polarization signal, which compares well with the theoretical maximum of 52% (data not shown).

3D ZF TEDOR allows all carbon$-$nitrogen distances to be measured simultaneously in a single 3D experiment. For the ith ^{13}C resonance located at frequency Ω_{C_i} in the direct dimension, a pattern of N_i cross-peaks emerges in the indirect dimension with increasing mixing time. Qualitatively, each (Ω_{N_j},Ω_{C_i}) cross-peak builds up at a rate which directly reflects the strength of the corresponding active dipolar coupling, ω_{ij}, and N_i provides information about the effective size of the ^{13}C$-^{15}$N spin cluster (i.e., number of ^{15}N spins simultaneously coupled to the ith ^{13}C spin, for which the ^{13}C$-^{15}$N couplings are sufficiently strong for the cross-peaks to be detectable experimentally). For the most accurate distance measurements, however, the dependencies on all interaction parameters included in eq 6, as well as the influence of relaxation and experimental imperfections, must be rigorously taken into account (see Internuclear Distance Measurements section below for details).

Although the 3D ZF TEDOR pulse sequence suppresses ^{13}C coherences responsible for artifacts in the 2D spectra, the distribution of the initial magnetization among multiple coherences reduces the amount of the available spin order that is stored in ^{13}C$-^{15}$N dipolar correlations. Quantitatively, this is described in eq 6 by the J-modulation of cross-peak intensities (contained in the $\cos^2(\pi J t_{\text{mix}}/2)$ terms), where the extent of the modulation for a particular ^{13}C site depends on the exact coupling topology (i.e., number of J-coupled ^{13}C spins and the corresponding coupling strengths). In Figure 2, we present a series of simulated TEDOR cross-peak buildup curves for a 50 Hz dipolar coupling (corresponding to a ^{13}C$-^{15}$N distance of 4 Å) and several J-coupling topologies typical for U-^{13}C-labeled peptides. The cross-peak intensities in the presence of J-couplings are found to be reduced approximately 2- to 5-fold for the various topologies investigated. As expected, the effects are the smallest for weakly J-coupled ^{13}C sites (e.g., side chain CH_3 groups) and most severe for strongly coupled sites (e.g., CO and C^α); this limits the range of ^{13}C$-^{15}$N dipolar couplings observable experimentally for strongly J-coupled ^{13}C nuclei by using 3D ZF TEDOR.

Homonuclear J-couplings can be suppressed in solid-state NMR experiments by using band-selective refocusing pulses as demonstrated previously,[42,43,54] and here we have adapted this J-decoupling strategy in the context of 3D TEDOR experiments. The resulting band-selective experiment (3D BASE TEDOR) shown in Figure 1b refocuses homonuclear J-couplings between ^{13}C spins within the selective pulse bandwidth and ^{13}C

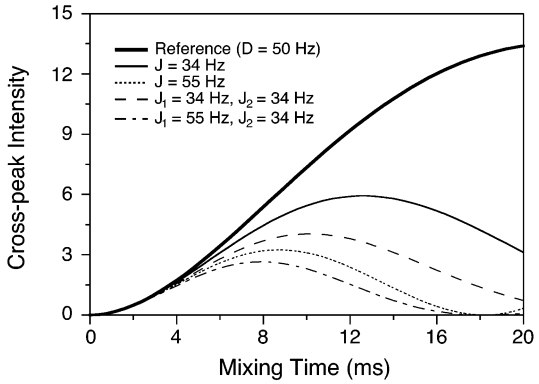

Figure 2. TEDOR cross-peak buildup curves simulated by using eq 6 for a $^{13}C-^{15}N$ spin pair with the dipolar coupling $D = 50$ Hz ($r = 4$ Å). The $^{13}C-^{15}N$ spin pair is considered to be either isolated (thick solid line) or in the presence of one or two additional *J*-coupled ^{13}C nuclei. For each coupling topology, the strengths of the $^{13}C-^{13}C$ *J*-couplings are given in the inset (values typical for U-^{13}C-labeled peptides were used), and the buildup curves were multiplied by $\exp(-\Gamma t_{mix})$, with $\Gamma = 50\ s^{-1}$, to model relaxation effects. For these and all other TEDOR buildup curves shown in this paper, the cross-peak intensities are given as a percentage of the ^{13}C signal in a reference one-dimensional cross-polarization experiment (i.e., $V(0) = 100$ in eq 6).

spins outside the bandwidth, and extends the range of $^{13}C-^{15}N$ distances that can be measured for strongly *J*-coupled ^{13}C sites. Assuming that $^{13}C-^{13}C$ *J*-couplings between nuclei within the selective pulse bandwidth are negligible, the REDOR mixing Hamiltonian is purely dipolar:

$$H = \sum_{j,k} \omega_{jk} 2I_{jz}S_{kz} \tag{7}$$

where the summation index j runs over ^{13}C spins inverted by the selective pulse. The cross-peak intensities are given by

$$V_{ij}(t_{mix}) = V_i(0)\langle \sin^2(\omega_{ij}t_{mix}/2) \prod_{k=1\neq j}^{N_i} \cos^2(\omega_{ik}t_{mix}/2)\rangle \tag{8}$$

where all terms have been defined in eq 6. We note that homonuclear *J*-decoupling is achieved at the expense of distance measurements being limited to those ^{13}C spins having resonance frequencies within the selective pulse bandwidth, which requires the acquisition of multiple 3D NMR spectra to cover the full ^{13}C spectral window.

Internuclear Distance Measurements. In principle, internuclear distances from the N_i ^{15}N nuclei dipolar coupled to the ith ^{13}C spin can be determined from the 3D ZF TEDOR experiment by fitting the buildup of cross-peaks located at $(\Omega_{N_k},\Omega_{C_i})$ in the 2D spectra, where $k = 1, 2, ..., N_i$, with a set of N_i equations of the form given in eq 6, which depend on N_i dipolar couplings and m_i *J*-couplings. For 3D BASE TEDOR the *J*-couplings can be neglected (see eq 8). In addition, parameters describing relaxation and experimental imperfections must be included in the simulations. The major difficulty associated with this approach is that the cross-peak buildup exhibits a formal dependence on the relative orientation of the N_i dipolar couplings. This would require the use of Euler angles describing the orientations of all dipolar tensors as additional fit parameters, which is impractical.

Instead, we use a simple analytical model to fit the cross-peak intensities and extract carbon−nitrogen distances. The approach is based on Bessel function expansions of dipolar-dephasing NMR signals derived by Mueller,[66] and it provides an approximate description of the TEDOR spin dynamics, which depends on dipolar coupling magnitudes alone and is free of geometric parameters. Below, we summarize the main features of the model and evaluate its utility for distance measurements by comparison with "exact" TEDOR cross-peak buildup simulations for an $I-S_2$ spin system.

As shown in detail by Mueller,[66] the cosine-modulated REDOR dipolar dephasing signal for individual crystallites in a powder sample can be written:

$$S_{REDOR}(t) = \cos(\omega t) = [J_0(\sqrt{2}Dt)]^2 + f(J_k(\sqrt{2}Dt),\beta,\gamma) \tag{9}$$

Here, ω is the orientation-dependent effective $^{13}C-^{15}N$ dipolar coupling reintroduced by the REDOR sequence (cf. eq 2), t is a generalized time variable, D is the dipolar coupling constant (cf. eq 3), $J_0(x)$ is a Bessel function of zeroth order, and $f(J_k(x),\beta,\gamma)$ is a complicated expression which depends on infinite series of Bessel functions, $J_k(x)$, and Euler angles, β and γ, describing the orientation of the dipolar tensor in the rotor-fixed reference frame. The first few terms of the Bessel function expansion provide an excellent description of the powder-averaged REDOR dephasing signal;[66] in fact, the $J_0(x)$ term alone gives a reasonable approximation. These observations are equally valid for TEDOR experiments.[66]

Utilizing such a zeroth-order approximation, we proceed to describe the 3D TEDOR experiments by neglecting all orientation dependent terms in eq 9. The resulting simulation model consists of a set of N_i equations, which are used to simultaneously fit the buildup of N_i cross-peaks corresponding to the ith ^{13}C nucleus:

$$\begin{aligned}
V_{i1}(t_{mix}) &= \\
&\Lambda_i(1 - [J_0(\sqrt{2}D_{i1}t_{mix})]^2) \prod_{k=2}^{N_i} (1 + [J_0(\sqrt{2}D_{ik}t_{mix})]^2) \\
V_{i2}(t_{mix}) &= \\
&\Lambda_i(1 - [J_0(\sqrt{2}D_{i2}t_{mix})]^2) \prod_{k=1\neq 2}^{N_i} (1 + [J_0(\sqrt{2}D_{ik}t_{mix})]^2) \\
&\vdots \\
V_{iN_i}(t_{mix}) &= \\
&\Lambda_i(1 - [J_0(\sqrt{2}D_{iN_i}t_{mix})]^2) \prod_{k=1}^{N_i-1} (1 + [J_0(\sqrt{2}D_{ik}t_{mix})]^2)
\end{aligned} \tag{10}$$

For 3D ZF TEDOR, the expression for Λ_i is given by

$$\Lambda_i = \frac{1}{2^{N_i}} V_i(0)\lambda_i \exp(-\Gamma_i t_{mix}) \prod_{l=1\neq i}^{m_i} \cos^2(\pi J_{il} t_{mix}/2) \tag{11}$$

whereas for the band-selective experiment, the *J*-coupling terms can be neglected:

$$\Lambda_i = \frac{1}{2^{N_i}} V_i(0)\lambda_i \exp(-\Gamma_i t_{mix}) \tag{12}$$

Most terms in eqs 10−12 have been defined in eqs 6 and 9.

(66) Mueller, K. T. *J. Magn. Reson. A* **1995**, *113*, 81−93.

Table 1. Carbon−Carbon *J*-Coupling Constants in *N*-acetyl-L-Val-L-Leu[a]

atoms		$^1J_{CC}$ (Hz)	atoms		$^1J_{CC}$ (Hz)
Ac(CO)	Ac(C^α)	51	Val(C^β)	Val($C^{\gamma 1}$)	35
Val(CO)	Val(C^α)	52	Val(C^β)	Val($C^{\gamma 2}$)	32
Leu(CO)	Leu(C^α)	61	Leu(C^β)	Leu(C^γ)	37
Val(C^α)	Val(C^β)	35	Leu(C^γ)	Leu($C^{\delta 1}$)	35
Leu(C^α)	Leu(C^β)	34	Leu(C^γ)	Leu($C^{\delta 2}$)	28

[a] Coupling constants were measured by using a two-dimensional spin−echo sequence described elsewhere.[42] In fitting the experimental *J*-dephasing curves, we assumed the contributions from $^2J_{CC}$ and weaker couplings to be negligible.

The relaxation of spin coherences due to insufficient proton decoupling is modeled as a single exponential with the relaxation rate, Γ_i. The constant, λ_i, describes the amplitude scaling of cross-peaks, which can arise from experimental imperfections, higher order CSA and $^{13}C-^{13}C$, $^1H-^{13}C$, and $^1H-^{15}N$ dipolar coupling effects, and possible systematic deviations associated with the description of experimental data using the approximate model (see discussion below). For the peptides investigated here, amplitude scaling factors were in the $\lambda = 0.5-1.0$ range, and typical relaxation rates were $\Gamma = 50-150\ s^{-1}$. The use of single λ_i and Γ_i parameters to fit all cross-peaks corresponding to the *i*th ^{13}C spin reduces the number of required fit parameters and is justified because the experimental and internal molecular parameters contributing to relaxation and amplitude scaling for each of the $(\Omega_{N_k},\Omega_{C_i})$ cross-peaks do not depend on whether a given $^{13}C-^{15}N$ coupling is active or passive (cf. eq 6). We note here that we have attempted to use separate two-dimensional spin−echo experiments with $^{13}C-^{13}C$ *J*-decoupling[42] to independently determine the ^{13}C relaxation rate, Γ. For the majority of ^{13}C sites in N-ac-VL, the spin−echo relaxation rates were found to be somewhat smaller than the values of Γ giving the best fits to cross-peaks observed in the 3D TEDOR experiments, and they can therefore be used to provide a lower bound for Γ.

In summary, the main features of the simulation model are the following: (i) for the *i*th ^{13}C nucleus coupled to N_i ^{15}N spins, all N_i $^{13}C-^{15}N$ distances are determined by simultaneously fitting the experimentally observed buildup of cross-peaks located at $(\Omega_{N_k},\Omega_{C_i})$, $k = 1, 2, ..., N_i$, using eqs 10−12 with $N_i + 2$ fit parameters (N_i dipolar coupling constants, D_{ik}, a relaxation rate, Γ_i, and an amplitude scaling factor, λ_i); (ii) no knowledge of dipolar tensor orientations and no powder averaging are required; and (iii) the cross-peak intensities at long mixing times are inversely proportional to the number of ^{15}N spins, N_i, simultaneously coupled to the ^{13}C nucleus, $V_{ik}(t_{mix}) \propto (2^{N_i})^{-1}$, which places a practical limit on the magnitude of the weakest $^{13}C-^{15}N$ couplings that can be determined by using 3D TEDOR methods (for the di- and tripeptides investigated in this work, $^{13}C-^{15}N$ dipolar couplings corresponding to distances in the 4−6 Å regime could be determined). We note that, for 3D ZF TEDOR, the buildup of cross-peaks for the *i*th ^{13}C nucleus also depends on the coupling topology of the m_i *J*-coupled ^{13}C nuclei (cf. eq 11). These parameters are held constant in the simulations since $^{13}C-^{13}C$ *J*-couplings in peptides do not vary significantly for different types of couplings (i.e., CO−C^α, $C^\alpha-C^\beta$, etc.).[52] We measured the $^{13}C-^{13}C$ *J*-couplings (see Table 1) in *N*-acetyl-L-Val-L-Leu and found them to be clustered closely around the reported average values.[52] For *N*-acetyl-L-Val-L-Leu cross-peak simulations, the experimentally determined *J*-couplings were used. For *N*-formyl-L-Met-L-Leu-L-Phe, the *J*-coupling constants were not explicitly determined, and in simulations we used the values $^1J_{CO-C^\alpha} = 55$ Hz and $^1J_{C^\alpha-C^\beta} = {}^1J_{C^\beta-C^\gamma} = {}^1J_{C^\gamma-C^\delta} = 34$ Hz.

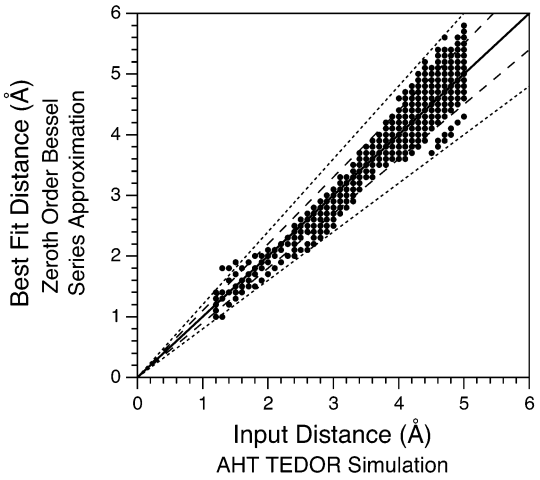

Figure 3. Comparison of the approximate simulation model with average Hamiltonian simulations for an $I-S_2$ spin system. A grid of TEDOR buildup curves based on average Hamiltonian theory was generated by using eq 8 for pairs of dipolar couplings with different magnitudes and relative orientations (see text for details). The AHT TEDOR simulations were subsequently fit by using the approximate analytical model in eq 10. Perfect agreement between the input distances used for the AHT calculations and best-fit distances obtained by using the approximate model is indicated by the solid line of slope 1.0. Discrepancies between the input and best-fit distances of ±10% and ±20% are indicated by the dashed and dotted lines, respectively.

Uncertainties in the Measured Distances. In the following section, we discuss the uncertainties in distances determined by using 3D TEDOR experiments. Specifically, we have investigated the errors due to (i) random noise, (ii) use of incorrect values of $^{13}C-^{13}C$ *J*-coupling constants in 3D ZF TEDOR simulations, and (iii) use of approximate analytical expressions in eqs 10−12 to model the cross-peak buildup. For the model peptides investigated here, we have found that carbon−nitrogen distances could be measured with a relative precision of approximately ±10−20%, where the uncertainty is mainly attributed to the use of the approximate simulation model.

The effects of random noise were evaluated by using a Monte Carlo approach.[67] For each set of N_i experimental cross-peak buildup curves corresponding to the *i*th ^{13}C spin, a large number of sets of buildup curves ($N \geq 1000$) were generated by adding to each mixing time point a random amount of noise with a Gaussian probability distribution (the width of the distribution was determined by the experimental signal-to-noise ratio measured from the 2D spectra). Each set of generated curves was subsequently fit by using a grid of simulated cross-peak buildup curves, where each curve in the grid was calculated as a function of the internuclear distances, relaxation rate, and scaling factor. The fitting was performed for the *N* random noise trials, and best-fit parameters for each trial were stored. The best-fit results for each trial were subsequently used to generate probability distribution plots for the different fit parameters; the final best-fit distances were extracted from the average of the distribution, and the width of the distribution provided a measure of the random error in the measured distances. The signal-to-

(67) Press, W. H.; Teukolsky, S. A.; Vetterling, W. T.; Flannery, B. P. *Numerical Recipes in C*; Cambridge University Press: Cambridge, 1996.

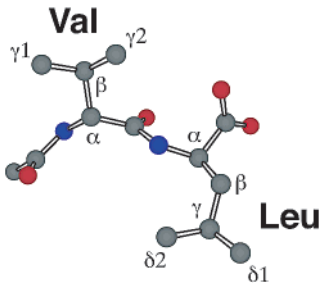

Figure 4. X-ray crystal structure of *N*-Acetyl-L-Val-L-Leu.[69]

noise ratio for the model peptides investigated here was relatively high, and for the majority of ^{13}C sites the errors in the measured distances due to random noise were found to be less than ±0.1 Å.

For 3D ZF TEDOR, the effect of using incorrect $^{13}C-^{13}C$ *J*-coupling constants (cf. eq 11) on the $^{13}C-^{15}N$ distance measurements was also investigated. For *N*-acetyl-L-Val-L-Leu, where the exact values of the *J*-couplings are known (see Table 1), we found that the best-fit distances were not appreciably affected when incorrect *J*-couplings (which differed by as much as ±25% from the actual values) were used in the simulations. Quantitatively, the differences in the best-fit $^{13}C-^{15}N$ distances were less than ±0.1 Å for distances in the 4 Å regime.

As noted above, the approximate model used to describe the buildup of cross-peaks in the 2D spectra is the main source of uncertainty in the $^{13}C-^{15}N$ distances measured by using 3D TEDOR experiments. To quantify these systematic errors, we have compared the approximate model described in eq 10 with "exact" powder-averaged simulations based on average Hamiltonian theory (AHT)[68] (see eq 8) for a model $I-S_2$ spin system. A grid of exact simulations was generated by using eq 8 for pairs of dipolar couplings with varying magnitudes and relative orientations. Specifically, the buildup curves were calculated

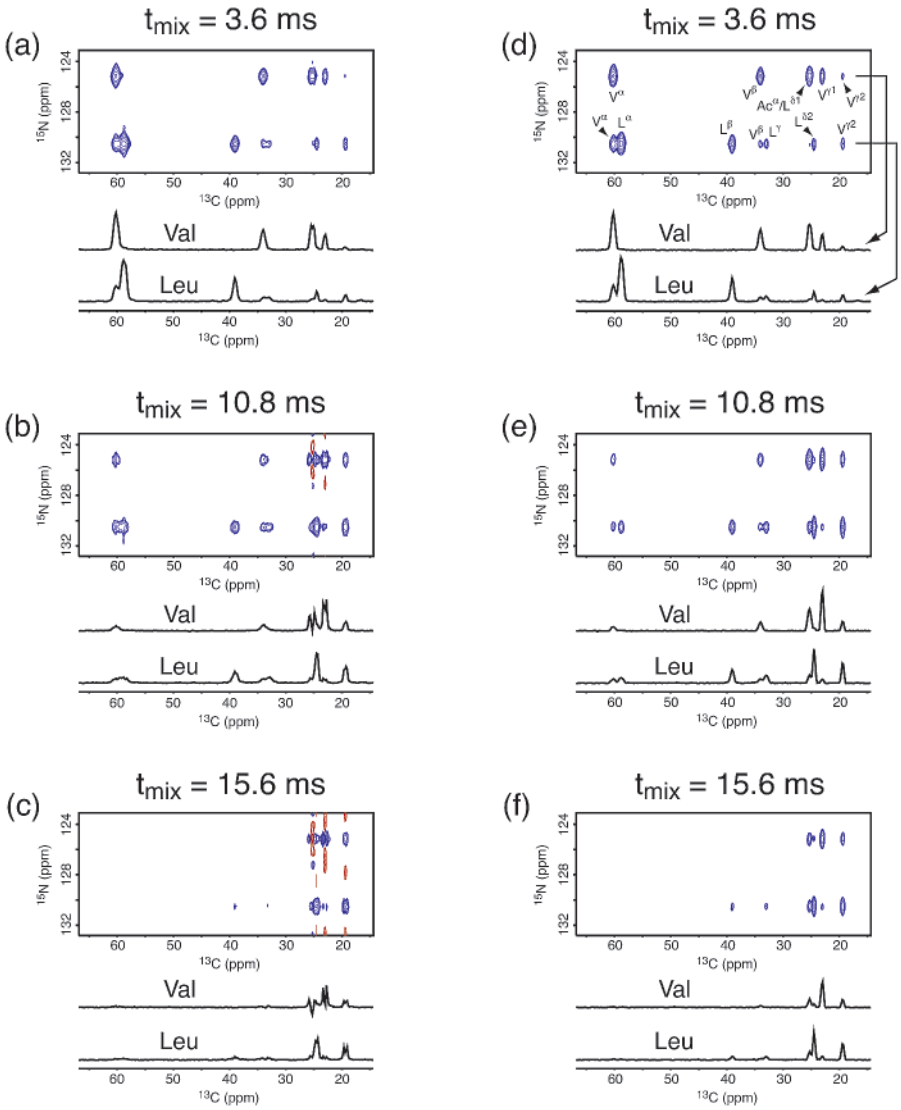

Figure 5. Representative two-dimensional slices from broadband 3D TEDOR experiments in [U-^{13}C,^{15}N]*N*-acetyl-L-Val-L-Leu. Spectra were recorded by using the pulse sequence in Figure 1a, without (a−c) and with (d−f) *z*-filters. The experiments demonstrate that the use of *z*-filters eliminates the detrimental effects of $^{13}C-^{13}C$ *J*-couplings and leads to pure absorption mode spectra (see text for details). Positive and negative contours are shown in blue and red, respectively. The experiments were performed at 500 MHz ^1H frequency, $\omega_r/2\pi = 10$ kHz ± 5 Hz, and *z*-filter delays of $\Delta = 200$ μs were used. Additional experimental parameters are described in the text. The 3D data set used to extract carbon−nitrogen distances was recorded by using the *z*-filtered sequence as (11, 1024, 16) points in (t_1, t_2, t_{mix}), with time increments of (2.0, 0.02, 1.2) ms, resulting in acquisition times of (20.0, 20.5, 18.0) ms. Each FID was 64 scans, the recycle delay was 3 s, and (t_1, t_2) points were acquired as complex pairs for phase-sensitive detection,[58] yielding a total measurement time of ~20 h.

for mixing times $t_{mix} = 0-20$ ms. Distances between 1.2 and 5.0 Å were used with a 0.1 Å increment, and for each pair of couplings the angle, θ, between the dipolar vectors was varied between 0° and 90° in 10° increments (the amplitude scaling factor and relaxation rate were set to $\lambda = 0.5$ and $\Gamma = 50$ s^{-1}, respectively, for the exact simulations). Subsequently, each exact simulation in the grid was fit by using a grid of approximate simulations generated by using eq 10 for distances in the 1.0−7.0 Å range, where the parameters λ and Γ were allowed to vary freely during the fit.

The results of fitting the exact AHT simulations by using the approximate analytical model are presented in Figure 3. Overall, the analytical model provides a good description of the spin dynamics in the $I-S_2$ system for the various coupling topologies (perfect agreement is indicated by the solid line of slope 1.0). For a given exact simulation input distance corresponding to the active dipolar coupling, the majority of best-fit distances obtained from the approximate simulations, which span a wide range of passive couplings and relative orientations, are well within ±10% of the input distance (indicated by the dashed lines), and virtually all best-fit distances are within ±20% of the input distance (indicated by the dotted lines). A closer examination of the results indicates that the approximate best-fit distances, which differ by more than 10% from the input distance used for the AHT simulation, correspond to a small subset of coupling topologies for which the two dipolar couplings are of similar magnitude and the angle between the dipolar vectors is in the $\theta = 0-20°$ range. This is consistent with previous observations.[24,35] The uncertainties of ±10−20% in the 3D TEDOR distance measurements are reasonable, and the utility of the simple analytical simulation model is further supported by good correspondence between the NMR and X-ray distances determined for the di- and tripeptides investigated here (see Results and Discussion section).

Finally, we note that the uncertainties in the distances measured by using 3D TEDOR experiments are somewhat larger than those obtained for frequency-selective REDOR measurements. For example, the error in a $^{13}C-^{15}N$ distance measured as 4.0 Å by using 3D TEDOR can be assumed to be in the ±0.4−0.8 Å range. By comparison, distances in the 4 Å regime measured by using FSR had typical uncertainties on the order of 0.1−0.2 Å.[43] The 3D TEDOR experiments, however, provide a more general approach to the determination of multiple structural constraints in uniformly ^{13}C,^{15}N-labeled systems.

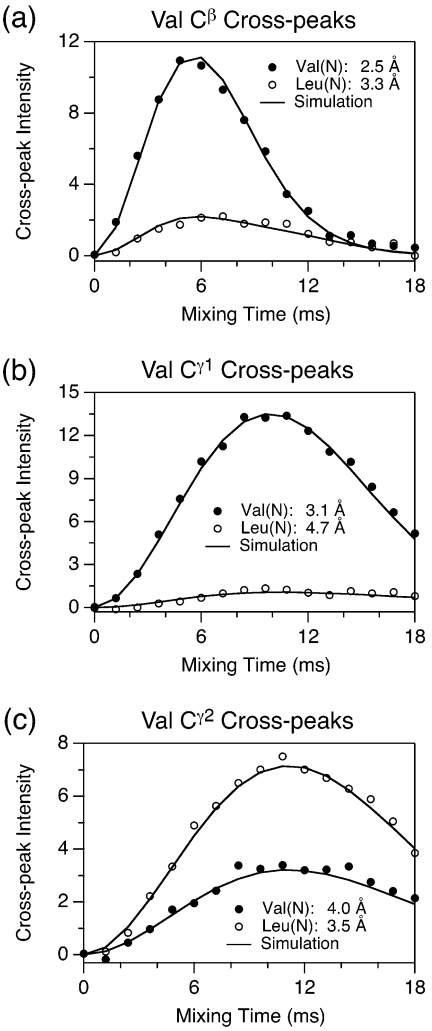

Figure 6. 3D ZF TEDOR cross-peak buildup curves in [U-^{13}C,^{15}N]*N*-acetyl-L-Val-L-Leu. The buildup curves were acquired by using the pulse sequence in Figure 1a and correspond to cross-peaks observed for the Val C^{β} (a), Val $C^{\gamma 1}$ (b), and Val $C^{\gamma 2}$ (c) resonances in the 2D correlation spectra in Figure 5d−f. For each ^{13}C, the experimental buildup curves corresponding to the Val (●) and Leu (○) ^{15}N sites were fit (−) by using analytical expressions in eq 10 based on the zeroth-order Bessel function approximation. The $^{13}C-^{13}C$ *J*-coupling constants used in the fits were measured in a separate experiment (see Table 1). The cross-peak buildup curves shown correspond to carbon−nitrogen distances in the 2.5−4.7 Å regime (the actual distances measured are noted in the insets). Similar simulations were performed for the remaining cross-peaks (cf. Figure 5), and the resulting $^{13}C-^{15}N$ internuclear distances are summarized in Table 2.

Results and Discussion

Distance Measurements in [U-^{13}C,^{15}N]*N*-Acetyl-Val-Leu. In the following we apply the 3D TEDOR experiments to the simultaneous measurement of multiple carbon−nitrogen distances in U-^{13}C,^{15}N-labeled peptides, *N*-acetyl-L-Val-L-Leu (N-ac-VL) and *N*-formyl-L-Met-L-Leu-L-Phe (N-f-MLF).

N-Acetyl-L-Val-L-Leu represents an excellent model system for the 3D TEDOR experiments. The three-dimensional structure of the peptide (see Figure 4) has been determined by using X-ray crystallography.[69] Furthermore, various SSNMR structural studies, which include complete ^{13}C and ^{15}N resonance assignments and carbon−nitrogen distance measurements,[43] have been performed for N-ac-VL.

In Figure 5, we show representative two-dimensional slices from the broadband 3D TEDOR experiments corresponding to mixing times in the range $t_{mix} \approx 4-16$ ms. The spectra in Figure 5a−c and 5d−f were acquired by using the pulse sequence in Figure 1a with the *z*-filter periods (highlighted by gray rectangles) omitted and included, respectively. For clarity, only the aliphatic ^{13}C resonances are shown, where the cross-peak assignments are based on previous studies.[43] While for short mixing times ($t_{mix} \approx 1-2$ ms), which reveal correlations between directly bonded ^{13}C and ^{15}N nuclei, the 2D spectra with and without the *z*-filter periods are nearly identical, for longer mixing times the spectra are clearly degraded due to $^{13}C-^{13}C$ *J*-evolution, as described in detail in the Appendix. The essential

(68) Haeberlen, U. *High-Resolution NMR in Solids: Selective Averaging*; Academic Press: New York, 1976.
(69) Carroll, P. J.; Stewart, P. L.; Opella, S. J. *Acta Crystallogr.* **1990**, *C46*, 243−246.

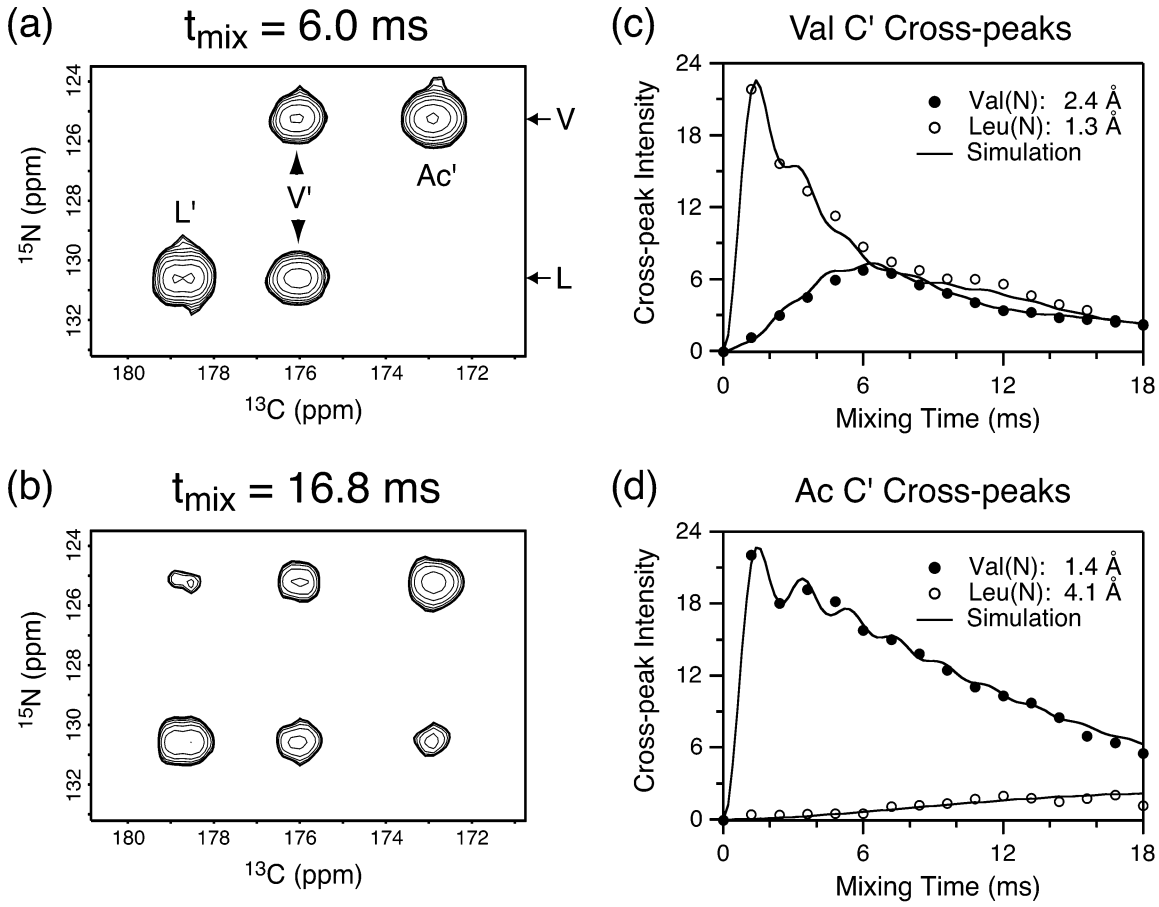

Figure 7. Representative two-dimensional slices from the 3D BASE TEDOR experiment for ^{13}CO nuclei and cross-peak buildup curves in [U-^{13}C,^{15}N]*N*-acetyl-L-Val-L-Leu. The pulse sequence in Figure 1b was used with the carrier placed in the carbonyl region and a Gausian band-selective ^{13}C refocusing pulse of 0.4 ms. Experimental parameters are described in the text, and the 3D data set was recorded as described in Figure 5. For the relatively short TEDOR mixing time (a), only the trivial one- and two-bond ^{13}C−^{15}N correlations are observed. However, with a longer mixing period (b), all cross-peaks expected in the CO region are detected (we note that cross-peaks corresponding to the weakest dipolar couplings were at the limit of detection when using the 3D ZF TEDOR sequence). The buildup curves for Val C′ (c) and Ac C′ (d) corresponding to the Val (●) and Leu (○) ^{15}N sites were fit (—) by using analytical expressions in eq 10, and the distances measured are found in the insets. All ^{13}C−^{15}N internuclear distances measured in N-ac-VL are summarized in Table 2.

spectral features due to the *J*-couplings in the form of spurious cross-peaks and phase-twisted lines are observed experimentally (Figure 5a−c). These artifacts can be suppressed by using the *z*-filter periods resulting in 2D spectra with pure absorption mode peaks (Figure 5d−f) and hence optimal resolution and sensitivity.

For *N*-acetyl-L-Val-L-Leu, a number of ^{13}C−^{15}N correlations are observed in Figure 5. Each cross-peak is labeled with the ^{13}C and ^{15}N frequencies characteristic of the dipolar coupled nuclei and can be used to obtain internuclear distance information. In Figure 6, we demonstrate the 3D TEDOR distance measurements from Val C$^{\beta}$ and both Val C$^{\gamma}$ carbons to the Val and Leu nitrogens. The cross-peak intensities, corresponding to carbon−nitrogen distances in the 2.5−4.7 Å range, are plotted in Figure 6a−c as a function of the TEDOR mixing time, t_{mix}. The internuclear distances were determined by fitting the experimental buildup curves using the analytical model described in the Theoretical Background section (cf. eq 10).

For ^{13}C nuclei having relatively strong *J*-couplings to other ^{13}C spins, such as CO and C$^{\alpha}$, cross-peaks corresponding to approximately 4 Å and longer distances were found to be at the limit of detection by using 3D ZF TEDOR, even for the simple spin system of two ^{15}N nuclei represented by *N*-acetyl-L-Val-L-Leu. Specifically, the Ac(C′)-Leu(N) and Leu(C′)-Val(N) cross-peaks had very poor signal-to-noise ratios, and the corresponding distances were difficult to quantify. Using the band-selective pulse sequence (3D BASE TEDOR) shown in Figure 1b, which refocuses the homonuclear *J*-couplings, cross-peaks corresponding to the weak dipolar couplings could

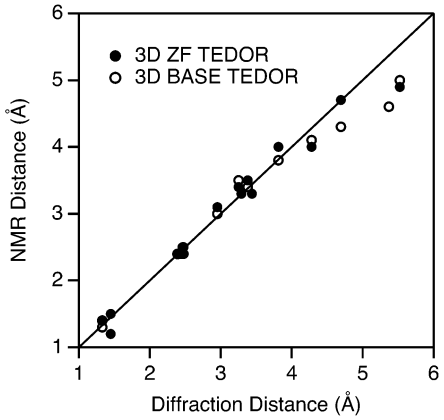

Figure 8. Comparison of carbon−nitrogen distances in *N*-acetyl-L-Val-L-Leu measured by using X-ray diffraction[69] and 3D ZF TEDOR (●) and 3D BASE TEDOR (○) experiments (see text for discussion of uncertainties in measured distances).

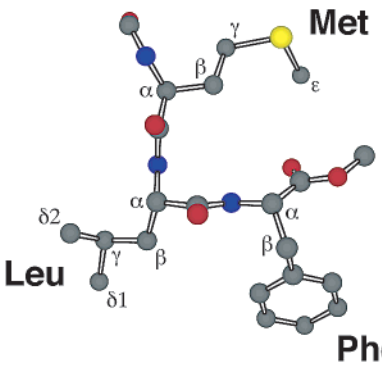

Figure 9. X-ray crystal structure of *N*-formyl-L-Met-L-Leu-L-Phe-OMe.[70]

be easily detected (Figure 7). Their buildup curves were used to measure the $^{13}C-^{15}N$ internuclear distances.

The carbon−nitrogen distance measurements in *N*-acetyl-L-Val-L-Leu are summarized in Figure 8 and Table 2. A total of 20 distances between ∼1.3 and 5 Å were measured in the peptide by using 3D ZF TEDOR and 3D BASE TEDOR. The measured distances are in good agreement with the X-ray crystal structure[69] and previous SSNMR studies.[43] Note that the slight systematic discrepancy between X-ray and NMR results for the longest distances measured ($r > \sim 4.5$ Å) is most likely caused by residual intermolecular dipolar couplings resulting from the insufficient dilution of [U-^{13}C,^{15}N]N-ac-VL in natural abundance N-ac-VL.

Distance Measurements in *N*-Formyl-[U-^{13}C,^{15}N]Met-Leu-Phe. *N*-Formyl-L-Met-L-Leu-L-Phe represents a more complicated spin system, where each ^{13}C can interact with up to three

Table 2. Internuclear Distances in *N*-Acetyl-L-Val-L-Leu

atoms		r_{C-N} (Å)[a] 3D ZF TEDOR	3D BASE TEDOR[b]	X-ray[c]
Val(N)	Ac(C′)	1.4	1.4	1.33
	Ac(C^{α})	2.4	2.4	2.39
	Val(C′)	2.4	2.4	2.39
	Val(C^{α})	1.5	−	1.45
	Val(C^{β})	2.5	−	2.46
	Val($C^{\gamma 1}$)	3.1	3.0	2.95
	Val($C^{\gamma 2}$)	4.0	3.8	3.81
	Leu(C′)	−	4.6	5.37
	Leu($C^{\delta 2}$)	4.9	5.0	5.52
Leu(N)	Ac(C′)	4.0	4.1	4.28
	Val(C′)	1.4	1.3	1.33
	Val(C^{α})	2.4	−	2.44
	Val(C^{β})	3.3	−	3.44
	Val($C^{\gamma 1}$)	4.7	4.3	4.69
	Val($C^{\gamma 2}$)	3.5	3.4	3.38
	Leu(C′)	2.4	2.5	2.47
	Leu(C^{α})	1.2	−	1.45
	Leu(C^{β})	2.4	−	2.48
	Leu(C^{γ})	3.3	−	3.29
	Leu($C^{\delta 2}$)	3.4	3.5	3.25

[a] See text for a detailed discussion of uncertainties associated with the NMR distance measurements. [b] Measurements of distances marked with a "−" for 3D BASE TEDOR were not attempted. [c] Reference 69.

^{15}N nuclei. Figure 9 shows the X-ray crystal structure of the methyl ester analogue of N-f-MLF, *N*-formyl-L-Met-L-Leu-L-Phe-OMe (N-f-MLF-OMe).[70] A number of $^{13}C-^{15}N$ distances in N-f-MLF were determined previously by using frequency-selective REDOR and found to be in good agreement with the corresponding distances in N-f-MLF-OMe.[43] In fact, the overall three-dimensional structure of N-f-MLF determined recently by

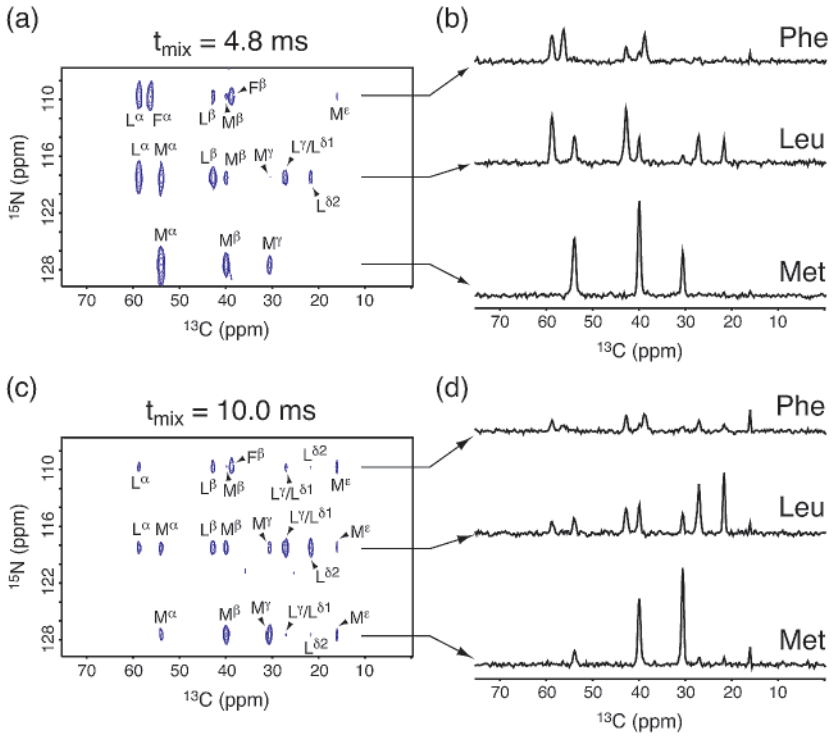

Figure 10. Representative two-dimensional slices for the 3D ZF TEDOR experiment in *N*-formyl-[U-^{13}C,^{15}N]L-Met-L-Leu-L-Phe. The 2D spectra shown in (a) and (c) (with the 1D slices corresponding to Met, Leu and Phe ^{15}N resonances shown in (b) and (d)) were recorded at 500 MHz ^{1}H frequency and $\omega_r/2\pi = 10$ kHz ± 5 Hz by using the pulse sequence in Figure 1a, with the *z*-filter delays of $\Delta = 200$ μs. Additional experimental parameters are described in the text. The 3D data set consisted of 16 2D spectra acquired for TEDOR mixing times up to 18 ms and incremented in a nonlinear fashion in order to maximize the information content and minimize the duration of the experiment. Each 2D spectrum was acquired as (19, 1024) complex points in (t_1, t_2), with time increments of (800, 20) μs, resulting in acquisition times of (14.4, 20.5) ms. Each FID was 128 scans, with a 3 s recycle delay, yielding a total measurement time of ∼67 h.

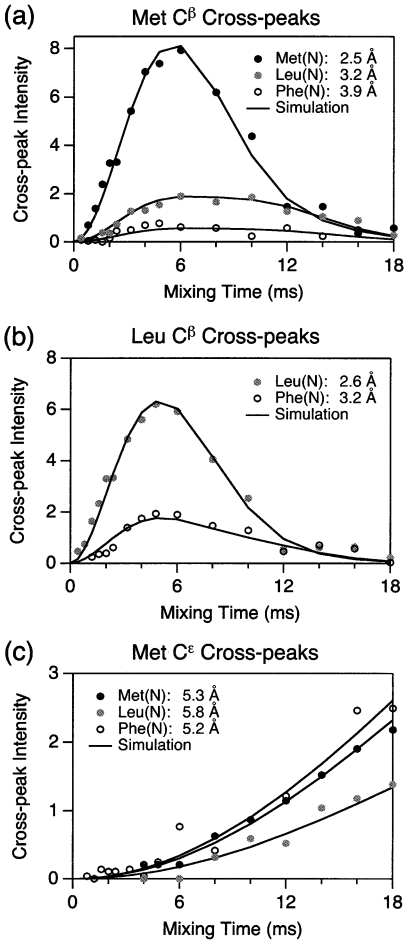

Figure 11. 3D ZF TEDOR cross-peak buildup curves in *N*-formyl-[U-^{13}C,^{15}N]L-Met-L-Leu-L-Phe. The buildup curves were acquired by using the pulse sequence in Figure 1a and correspond to cross-peaks observed for the Met C$^{\beta}$ (a), Leu C$^{\beta}$ (b), and Met C$^{\epsilon}$ (c) resonances in the 2D correlation spectra in Figure 10. For each ^{13}C, the experimental buildup curves corresponding to the Met (solid circles), Leu (gray circles), and Phe (open circles) ^{15}N sites were fit (—) by using analytical expressions in eq 10 based on the zeroth-order Bessel function approximation. The values of ^{13}C−^{13}C *J*-coupling constants used in the fits were 55 Hz for $^{1}J_{CO-C^{\alpha}}$ and 34 Hz for all other *J*-couplings. The cross-peak buildup curves shown in the figure correspond to carbon−nitrogen distances in the 2.5−5.8 Å regime (actual distances measured are found in the insets). Similar simulations were performed for the remaining cross-peaks (cf. Figure 10), and the ^{13}C−^{15}N internuclear distances are summarized in Table 3.

using SSNMR methods[49] is in close agreement with the N-f-MLF-OMe X-ray structure.

Figure 10 shows representative 2D ^{15}N−^{13}C correlation spectra in *N*-formyl-[U-^{13}C,^{15}N]L-Met-L-Leu-L-Phe recorded by using 3D ZF TEDOR. A large number of dipolar correlations (∼20) are observed in the aliphatic ^{13}C region for the spectrum acquired with 10 ms of TEDOR mixing (Figure 10c), and each cross-peak carries information about ^{13}C−^{15}N internuclear distances. The ^{13}C and ^{15}N resonance assignments for N-f-MLF have been presented in previous studies.[4,43,71] The 3D ZF TEDOR cross-peak buildup curves for selected ^{13}C sites corresponding to distances in the 2.5−5.8 Å range are shown in Figure 11.

(70) Gavuzzo, E.; Mazza, F.; Pochetti, G.; Scatturin, A. *Int. J. Pept. Protein Res.* **1989**, *34*, 409−415.
(71) Hong, M.; Griffin, R. G. *J. Am. Chem. Soc.* **1998**, *120*, 7113−7114.

Table 3. Internuclear Distances in *N*-Formyl-L-Met-L-Leu-L-Phe

atoms		r_{C-N} (Å)[a] 3D ZF TEDOR	3D BASE TEDOR[b]	X-ray[c]
Met(N)	Met(C′)	−	2.5	2.40
	Met(C$^{\alpha}$)	1.5	−	1.46
	Met(C$^{\beta}$)	2.5	2.6	2.50
	Met(C$^{\gamma}$)	3.8	−	3.04
	Met(C$^{\epsilon}$)	5.3	−	5.71
	Leu(C$^{\delta 2}$)	6.1	−	6.28
Leu(N)	Met(C′)	−	1.3	1.33
	Met(C$^{\alpha}$)	2.6	−	2.44
	Met(C$^{\beta}$)	3.2	3.2	3.20
	Met(C$^{\gamma}$)	5.0	−	4.56
	Met(C$^{\epsilon}$)	5.8	−	5.93
	Leu(C′)	−	2.4	2.46
	Leu(C$^{\alpha}$)	1.5	−	1.46
	Leu(C$^{\beta}$)	2.6	2.6	2.50
	Leu(C$^{\delta 2}$)	3.9	−	3.63
Phe(N)	Met(C′)	−	3.4	3.41
	Met(C$^{\beta}$)	3.9	3.8	4.06
	Met(C$^{\gamma}$)	5.6	−	5.43
	Met(C$^{\epsilon}$)	5.2	−	5.62
	Leu(C′)	−	1.3	1.34
	Leu(C$^{\alpha}$)	2.3	−	2.43
	Leu(C$^{\beta}$)	3.2	3.1	3.12
	Leu(C$^{\delta 2}$)	6.0	−	5.38
	Phe(C′)	−	2.7	2.37
	Phe(C$^{\alpha}$)	1.4	−	1.47
	Phe(C$^{\beta}$)	2.6	2.6	2.53

[a] See text for a detailed discussion of uncertainties associated with the NMR distance measurements. [b] Measurements of distances marked with a "−" for 3D BASE TEDOR were not attempted. [c] Reference 70.

The 3D BASE TEDOR experiment is demonstrated in Figure 12 for distance measurements in N-f-MLF involving ^{13}CO sites. Here, the dipolar coupling between Met(C′) and Phe(N) is of most interest. It corresponds to an internuclear distance of 3.4 Å and provides direct information about backbone conformation. The Met(C′)-Phe(N) cross-peak (at the limit of detection using 3D ZF TEDOR) is easily detected (Figure 12b), and its buildup can be used to determine the internuclear distance (Figure 12c).

The carbon−nitrogen distance measurements in *N*-formyl-L-Met-L-Leu-L-Phe are summarized in Figure 13 and Table 3. A total of 26 distances between ∼1.3 and 6 Å were measured in N-f-MLF by using 3D ZF TEDOR and 3D BASE TEDOR. The measured distances are in good agreement with the corresponding X-ray diffraction distances in N-f-MLF-OMe[70] and previous SSNMR studies.[43] We note here that, for demonstration purposes, we have applied 3D BASE TEDOR to distance measurements involving ^{13}C resonances other than ^{13}CO in both peptides (buildup curves are not shown). The ^{13}C−^{15}N distances measured by using the band-selective experiments in the methyl region of N-ac-VL and the C$^{\beta}$ region in N-f-MLF corresponded closely to the distances determined by using 3D ZF TEDOR (see Tables 2 and 3).

Finally, we note that many dipolar couplings measured in N-ac-VL and N-f-MLF by using the 3D TEDOR techniques corresponded to the trivial one- and two-bond ^{13}C−^{15}N distances, which do not restrain the peptide structure, and served as control experiments. In N-ac-VL, 10 structurally interesting distances ($r > \sim 3$ Å) were measured, and in N-f-MLF, 13 such distances were determined. A number of distances in the 3−4 Å regime (e.g., Val(C$^{\beta}$)-Leu(N), Val(C$^{\gamma 1}$)-Val(N), and Leu(C$^{\gamma}$)-Leu(N) in N-ac-VL; Met(C$^{\beta}$)-Leu(N), Met(C$^{\gamma}$)-Met(N), and Leu(C$^{\beta}$)-Phe(N) in N-f-MLF) depend on a single ψ or χ torsion

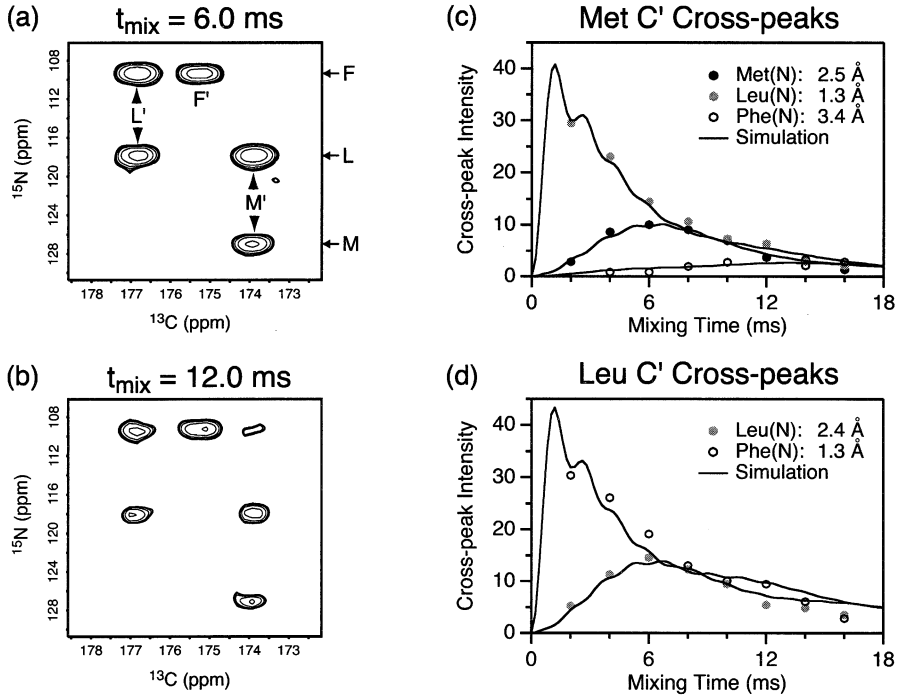

Figure 12. Representative two-dimensional slices from the 3D BASE TEDOR experiment for ^{13}CO nuclei and cross-peak buildup curves in *N*-formyl-[U-^{13}C,^{15}N]L-Met-L-Leu-L-Phe. The pulse sequence in Figure 1b was used with the carrier frequency on resonance with the carbonyl region of the spectrum and a Gausian band-selective ^{13}C refocusing pulse of 0.4 ms. Experimental parameters are described in the text. The 3D data set was recorded as (12, 1024, 8) points in (t_1, t_2, t_{mix}), with time increments of (0.8, 0.02, 2.0) ms, resulting in acquisition times of (8.8, 20.5, 16.0) ms. Each FID was 256 scans, the recycle delay was 3 s, and (t_1, t_2) points were acquired as complex pairs, yielding a total measurement time of ~42 h. The buildup curves for Met C′ (c) and Leu C′ (d) corresponding to the Met (solid circles), Leu (gray circles), and Phe (open circles) ^{15}N sites were fit (—) by using analytical expressions in eq 10, and the distances determined are indicated in the insets. All ^{13}C−^{15}N internuclear distances measured in N-f-MLF are summarized in Table 3.

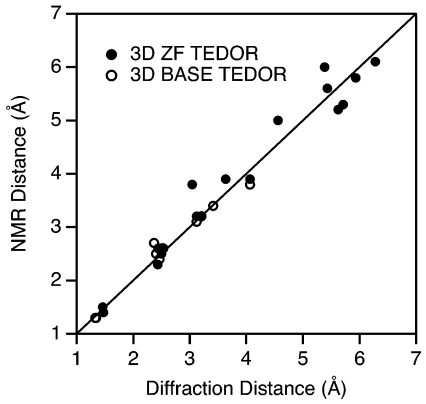

Figure 13. Comparison of carbon−nitrogen distances in *N*-formyl-L-Met-L-Leu-L-Phe measured by using 3D ZF TEDOR (●) and 3D BASE TEDOR (○) with the corresponding X-ray diffraction distances determined for N-f-MLF-OMe[70] (see text for discussion of uncertainties in measured distances).

angle, and the longer distances in the 4−6 Å range contain information about multiple ϕ, ψ, and χ torsion angles. These ^{13}C−^{15}N distance measurements place very strong constraints on the overall peptide structure (particularly on the side chain conformations), but in general they should be used in combination with other structure determination methods, such as chemical shift assignments, and direct measurements of torsion angles, to uniquely define a three-dimensional peptide structure. This approach was used for N-f-MLF, where long-range ^{13}C−^{15}N distance measurements[43] were combined with measurements of 10 ϕ, ψ, and χ torsion angles from dipolar tensor correlation experiments[48] and used as constraints in the calculation of a three-dimensional SSNMR structure for the tripeptide.[49]

Conclusions

In conclusion, we have presented two 3D TEDOR NMR experiments for the simultaneous measurement of multiple carbon−nitrogen distances in uniformly ^{13}C,^{15}N-labeled solids in site-specific fashion. The novel feature of the experiments is that they are specifically compensated for the detrimental effects of ^{13}C−^{13}C *J*-couplings on the measurements of long-range carbon−nitrogen distances. The experiments are robust and straightforward to implement. Qualitatively, the ^{13}C−^{15}N correlations in themselves provide direct information about three-dimensional structure, and quantitative distance measurements were performed by using a simple analytical simulation model, which accounts explicitly for multiple spin−spin couplings contributing to cross-peak buildup. The utility of the experiments for structural studies was demonstrated by measurements of 20 and 26 carbon−nitrogen distances up to ~5−6 Å in two uniformly ^{13}C,^{15}N-labeled peptides. Specifically, 10 ^{13}C−^{15}N distances measured in N-ac-VL and 13 distances in N-f-MLF are greater than 3 Å and provide valuable structural constraints. We expect the 3D TEDOR experiments demonstrated here on microcrystalline peptides to be applicable to structural measurements in noncrystalline biological systems, such as amyloid fibrils and membrane proteins. We have recently used 3D ZF TEDOR to simultaneously measure multiple ^{13}C−^{15}N distances in the 3−5 Å range in a U-^{13}C,^{15}N-labeled amyloid fibril-forming peptide, and applications to distance measurements in the bacteriorhodopsin active site[47] can be envisaged.

Acknowledgment. The authors thank Dr. Vladimir Ladizhansky, Dr. Chad Rienstra, Dr. David Ruben, and Dr. Jonathan Lansing for stimulating discussions during the course of this work, and Dr. Bernd Reif for a careful reading of the manuscript. C.P.J. thanks the NSF for a Predoctoral Fellowship. This research was supported by NIH Grants GM-23403, GM-23289, and RR-00995.

Appendix

In this section we calculate the 3D TEDOR spin dynamics in the simplest multiple-spin system (I_2-S) having heteronuclear dipolar and homonuclear *J*-couplings. Although this is much simpler than the spin systems represented by the uniformly ^{13}C,^{15}N-labeled peptides, it is sufficient to demonstrate the detrimental effects due to homonuclear *J*-couplings and explain the main features observed in the experimental 2D correlation spectra shown in Figure 5a−c. We consider the 3D TEDOR pulse sequence shown in the Figure 1a, where the *z*-filter periods, Δ, are set to zero (i.e., the homonuclear *J*-coupling is active throughout the entire experiment). In the analysis, it is sufficient to follow the evolution of the transverse magnetization corresponding to one of the spins, for instance I_{1x}. The results can be extended to the second spin by simply interchanging the labels 1 and 2. For consistency, in the following derivations we use the notation introduced in eqs 1−5 of the Theoretical Background section.

For the model I_2-S spin system, the effective Hamiltonian during the REDOR mixing periods is given by

$$H = \sum_{k=1,2} \omega_k I_{kz} S_z + \pi J 2 I_{1z} I_{2z} \tag{A1}$$

Therefore, after the first REDOR mixing period followed by the 90° pulses applied on the *I* and *S* channels, I_{1x} transforms to

$$I_{1x} \rightarrow (I_{1x} c_J - 2 I_{1z} I_{2y} s_J) c_{\omega 1} - 2(I_{1z} c_J + 2 I_{1x} I_{2y} s_J) S_y s_{\omega 1} \tag{A2}$$

The applied phase cycle eliminates all coherences which contain only *I*-spin operators after the first REDOR mixing period, and retains terms which depend on transverse *S*-spin operators:

$$I_{1x} \rightarrow -2(I_{1z} c_J + 2 I_{1x} I_{2y} s_J) S_y s_{\omega 1} \tag{A3}$$

Thus, in addition to the desired anti-phase coherence ($\sim I_{1z} S_y$), which reflects $I-S$ dipolar correlations and carries $I-S$ distance information, an additional term ($\sim I_{1x} I_{2y} S_y$) is also generated, which depends on $I-I$ correlations and is represented by a combination of zero-quantum (ZQ) and double-quantum (DQ) spin coherences with respect to *I*-spin operators.

The REDOR excitation is followed by a free evolution period (t_1) under the Hamiltonian

$$H = \sum_{k=1,2} \Omega_{Ik} I_{kz} + \Omega_S S_z + \pi J 2 I_{1z} I_{2z} \tag{A4}$$

This leads to

$$\begin{aligned} I_{1x} \rightarrow & -2 I_{1z} S_y s_{\omega 1} c_J \cos(\Omega_S t_1) \\ & - Z Q_x S_x s_{\omega 1} s_J \{\cos[(\Omega_{I1} - \Omega_{I2} + \Omega_S) t_1] - \cos[(\Omega_{I1} - \Omega_{I2} - \Omega_S) t_1]\} \\ & + Z Q_y S_y s_{\omega 1} s_J \{\cos[(\Omega_{I1} - \Omega_{I2} + \Omega_S) t_1] + \cos[(\Omega_{I1} - \Omega_{I2} - \Omega_S) t_1]\} \\ & + D Q_x S_x s_{\omega 1} s_J \{\cos[(\Omega_{I1} + \Omega_{I2} + \Omega_S) t_1] - \cos[(\Omega_{I1} + \Omega_{I2} - \Omega_S) t_1]\} \\ & + D Q_y S_y s_{\omega 1} s_J \{\cos[(\Omega_{I1} + \Omega_{I2} + \Omega_S) t_1] + \cos[(\Omega_{I1} + \Omega_{I2} - \Omega_S) t_1]\} \end{aligned} \tag{A5}$$

where we have retained only the cosine-modulated chemical shift terms, and the following notation for the ZQ and DQ coherences was used:[52]

$$\begin{aligned} Z Q_x &= I_{1x} I_{2x} + I_{1y} I_{2y}, \quad Z Q_y = I_{1y} I_{2x} - I_{1x} I_{2y} \\ D Q_x &= I_{1x} I_{2x} - I_{1y} I_{2y}, \quad D Q_y = I_{1x} I_{2y} + I_{1y} I_{2x} \end{aligned} \tag{A6}$$

The $I_{1z} S_y$ coherence in eq A5 is modulated by the *S*-spin chemical shift, Ω_S, and gives rise to the desired cross-peaks located at (Ω_S,Ω_I) in the 2D spectra. The zero- and double-quantum coherences evolve in the indirect dimension with frequencies $\Omega_{1I} \pm \Omega_{2I} \pm \Omega_S$, giving rise to spurious cross-peaks. For the simple I_2-S spin system, only the isotropic chemical shift terms in the Hamiltonian in eq A4 contribute to the spin dynamics during t_1. For larger spin systems having multiple $I-I$ *J*-couplings, the scalar interactions would also contribute to the evolution, resulting in more complicated dynamics.

The second pair of 90° pulses followed by the REDOR mixing period generates *I*-spin coherences, which are subsequently detected during the acquisition of the FID in t_2. The coherences are represented by both in-phase ($\sim I_x$) and anti-phase ($\sim I_y I_z$) terms:

$$\begin{aligned} I_{1x} \rightarrow & -(I_{1x} c_J^2 - 2 I_{1y} I_{2z} s_J c_J) s_{\omega 1}^2 \cos(\Omega_S t_1) \\ & - (I_{1x} c_J^2 + 2 I_{1y} I_{2z} s_J c_J) s_{\omega 1}^2 \{\cos[(\Omega_{I1} - \Omega_{I2} + \Omega_S) t_1] + \cos[(\Omega_{I1} - \Omega_{I2} - \Omega_S) t_1]\} \\ & - (I_{2x} c_J^2 + 2 I_{2y} I_{1z} s_J c_J) s_{\omega 1} s_{\omega 2} \{\cos[(\Omega_{I1} - \Omega_{I2} + \Omega_S) t_1] - \cos[(\Omega_{I1} - \Omega_{I2} - \Omega_S) t_1]\} \end{aligned} \tag{A7}$$

Under the chemical shift and homonuclear *J*-coupling interactions, the in-phase terms ($\sim I_x$) in eq A7 give rise to purely absorptive doublets split by the *J*-coupling,

$$I_{1x} \rightarrow I_{1+} (e^{i(\Omega_{I1} - J/2) t_2} + e^{i(\Omega_{I1} + J/2) t_2}) \tag{A8}$$

while the anti-phase terms ($\sim I_y I_z$) generate purely dispersive doublets with anti-phase components:

$$2 I_{1y} I_{2z} \rightarrow i I_{1+} (e^{i(\Omega_{I1} - J/2) t_2} - e^{i(\Omega_{I1} + J/2) t_2}) \tag{A9}$$

The superposition of these signals results in phase-twisted lines in the direct dimension and prohibits the extraction of reliable cross-peak intensities.

In summary, even for relatively simple multiple-spin systems, the presence of homonuclear *J*-couplings leads to quite com-

plicated spin dynamics. The *J*-couplings generate artifacts in the 2D correlation spectra in the form of spurious cross-peaks and phase-twisted lines, which degrade the resolution and prohibit the extraction of reliable cross-peak intensities. The *J*-coupling effects become more severe as the mixing time increases, since the anti-phase components are modulated by $\sin(\pi J t_{mix}/2)$. This is clearly a problem for the measurements of weak dipolar couplings, which typically employ relatively long mixing times.

The modified 3D TEDOR pulse sequences presented here make use of *z*-filter periods and band-selective refocusing pulses to suppress the ZQ and DQ spin coherences and refocus the *J*-couplings altogether, respectively. Both experiments generate pure absorption mode 2D spectra, where the cross-peaks located at (Ω_S,Ω_I) depend primarily on dipolar $I-S$ correlations and can be used to determine internuclear distances.

JA026385Y